BSPE9830U-2081-1

남해역 최외곽 (무인)도서 주변 해역의 종합 해양과학 조사와 통합적 관리방안 수립 연구에 관한 예비 기획연구

2009. 6

한 국 해 양 연 구 원

BSPE9830U-2081-1

남해역 최외곽 (무인)도서 주변 해역의 종합 해양과학 조사와 통합적 관리방안 수립 연구에 관한 예비 기획연구

2009. 6

한 국 해 양 연 구 원

제 출 문

한국해양연구원장 귀하

본 보고서를 “한국해양연구원 창의과제 사업(08년도)”의 최종보고서로 제출합니다.

2009. 6

연구기관명: 한국해양연구원
연구책임자: 임동일
연구원 : 김소영, 강소라

목 차

Chapter I. 기획연구 (남해역 최외곽 (무인)도서 주변 해역의 종합 해양과학 조사와 통합적 관리방안 수립 연구에 관한 예비 기획연구)

Chapter II

Chapter I. 기획연구

남해역 최외곽 (무인)도서 주변 해역의 종합
해양과학 조사와 통합적 관리방안 수립
연구에 관한 예비 기획연구

1. 추진 필요성 및 목적

1.1. 추진 필요성

추진필요성

☐ 해양영토관리, 기후변화, 해양환경보전 등의 국가적 현안을 해결하기 위한 최외곽 및 전략 (무인)도서와 주변 해양환경/생태 조사 및 이용/보전/관리 방안 도출이 필요함.

☐ 도서(섬)는 실효적 지배와 이용정도에 따라 중요한 영토학장 즉 해양 경계 획정의 기준이 되는 기선 기준점(영해기점 무인도서)임. 따라서 해양영토 관리를 위해 영해기점 도서, 최외곽 도서 등에 대한 과학적인 지리정보 자료 구축과 국가 정책 도출이 필요함.

☐ 남해역 최외곽 (무인)도서 주변 해역은 우리나라에서 전지구적 지구온난화 영향의 최전선 해역임. 특히 건강한 생태계를 유지하고 있어 기후변화나 환경변화에 매우 민감하게 반응할 것으로 예측되며, 그 결과 다양한 고감도 기후변화 생물상 연구가 용이함. 따라서 기후변화를 감시하기위한 최적의 모니터링 해역으로 평가됨.

☐ 남해역의 (무인)도서 주변 해역은 상대적으로 인간의 간섭이 적어 생물학적, 환경학적, 생태학적, 해양자원 및 관광학적 가치가 매우 높고, 도서마다의 독특하고 고유한 지형/지질/환경/생태 특성을 유지하고 있어 보전/관리 방안이 필요함.

※ 남해는 다도해(전국 무인도서: 2,679개, 남해역의 무인도서: 약 2,034개)로 남해 전 해역의 해양환경/생태계가 이들 도서(섬)들의 환경/생태계에 의해 조절될 정도로 무인도서가 남해역의 해양생태계를 조절하는 생태축(한반도 3대 생태축: 백두대간 생태축, 비무장지대 생태축, 도서 및 연안지역의 생태축)으로, 일종의 "해상그린벨트" 역할을 담당함. 따라서 무인도서는 생태계의 박물관으로 보존의 가치가 매우 큼.

※ 무인도서는 이동성 해양포유류, 어류 등의 중간기착지, 서식지 역할을 하며, 수심이 깊은 바다 한가운데서 생산성이 높은 연안역을 형성하며 바다의 오아시스와 같은 기능을 수행.

※ 무인도서 주변해역의 해양생태계는 육지에 가까운 연안해역의 생태계와는 기능과 구조가 다른 보존가치가 높은 환경임에도 불구하고 기존에 시행된 무인도서 자연환경조사는 도서의 육상생태계에만 초점. 따라서 생물 다양성이 매우 높고, 건강한 환경/생태계를 유지하고 있는 무인도서 주변 해양생태를 보전/관리할 필요가 있음.

◎ 남해역 무인도서 연구의 법적 타당성

※무인도서의 보전 및 관리에 관한 법률(2007. 08): 해양수산부장관은 무인도서 및 그 주변해역의 효율적인 보존·관리를 위하여 무인도서 및 그 주변해역에 대한 종합정보체계를 구축·운영할 수 있다.

※해양수산부 장관은 무인도서의 효율적인 관리를 위하여 5년마다 무인도서에 대한 실태조사를 실시하여야 한다.
(독도 등 도서지역의 생태계보전에 관한 특별법에 따라 특성도서로 지정된 도서는 이 법의 적용을 받지 아니한다. 예) 전국무인도서자연환경조사사업에 의해 지정된 특정도서)

※남해연구소가 수행해야 할 당위성: 남해의 대표적 특성인 다도해→각 무인도서마다 갖고 있는 독특한 환경/생태 특성 연구 필요→남해특성연구부의 연구기능인 남해권역의 환경 특성 연구와 연관됨.

◎ 무인도서 현황

전국 무인도서는 총 2,679개의 총 면적 약 3,800km^{2}임(아래 표 참조). 무인도서의 자연환경은 인간의 간섭이 적어 안정된 생태계를 유지하고 있으며, 내륙과 달리 지역 고유종이 풍부하고, 식생구계학적으로 중요한 난대성 식물군락이 존재하며, 멸종위기야생동·식물 및 희귀동야생식·물의 서식지·번식지(특히 멸종위기 조류의 집단서식지)이며, 독특한 자연경관을 유지하고 있어 다른 어느 곳보다 보전가치가 높음. 하지만 무인도의 경우 일부 학술조사 이외에 종합적이고 체계적인 조사·연구가 전무하고, 관리부재로 수석용 돌·분재용 식물의 무분별한 채취가 만연하고 있으며, 염소등 가축의 방목으로 생태계가 교란되고 있으나 현재 무인도서에 대한 관리는 체계적이지 못함.

구분	도 서 수			면 적 (㎢)		
	계	유인도	무인도	계	유인도	무인도
총 계	3,170	491	2,679	3,786	3,701	85.3
부산광역시	41	3	38	38	35	3.3
인천광역시	154	42	112	647	641	6.1
울산광역시	4	0	4	0.04	0	0.04
경기도	65	11	54	45	44	0.8
강원도	32	0	32	0.3	0	0.3
충청남도	261	37	224	163	150	12.5
전라북도	109	26	83	38	35	2.6
전라남도	1,969	280	1,689	1,856	1,810	45.9
경상북도	47	4	43	74	74	0.1
경상남도	425	80	345	910	898	11.8
제주도	63	8	55	15	14	1.7

◎ 무인도서의 자연환경 특징

○ 인간의 간섭이 적은 안정된 생태계 유지 (생태계의 박물관)

○ 내륙과 달리 지역 고유종 풍부

○ 식생구계학적으로 중요한 난대성 식물군락 존재

○ 멸종위기야생동·식물 및 희귀동야생식·물의 서식지·번식지

○ 독특한 자연경관 유지

◎ 무인도서 관리의 문제점 (해양수산부, 2005, 무인도서 실태조사 및 통합적 관리 방안, 307p)

○ 도서 생태계에 대한 체계적이고 종합적인 조사·연구자료 부족

○ 쓰레기와 외부간섭으로 인한 생태계 훼손(수석용 돌·분재용 식물의 무분별한 채취, 가축의 방목 등)과 교란 심화

○ 영토관리를 위한 영해기점 도서 및 최외곽 도서/암초에 대한 정보 부족과 이를 보호하기 위한 법적 흠결

○ 무인도서 및 주변 해역의 난개발 방지와 이용/개발수요의 합리적 수

용을 위한 정책수단 미비

- 무인도서 주변 지역주민과 방문객에 대한 교육홍보 미흡
- 국토자원으로 무인도서 관리정책 부재

◎ 무인도서 통합적 관리 기본정책 방향 (해양수산부, 2005, 무인도서 실태조사 및 통합적 관리 방안, 307p)

- 해양수산부의 보고에 따르면, 무인도서의 통합적 관리 기본정책방향은 “육지부와 해면부, 관련 부처 이해당사자, 보전과 이용/개발 사이의 조정과 통합의 정책메커니즘을 구축하여, 무인도서를 활용한 국가의 부가가치 창출 극대화”로 설정할 수 있음.
- 무인도서 통합적 관리 기본정책 방향을 위한 관리체계 개선 방안은 “정책수요 충족을 위한 무인도서 관리개념 정립”, “무이도서 관리주체 정립”, “무인도서 유형구분 및 유형별 관리방안”, “자연환경 및 인문사회현황 종합실태조사”, “무인도서의 환경친화적 이용 및 개발실현”, “무인도서 관리프로세스 개선” 6가지로 제시됨.

1.2. 목적

목적

□ 남해역 최외곽 및 전략 (무인)도서 및 주변 해역에 대한 체계적이고 종합적인 해양과학 조사-연구를 통한 해양환경 보전, 기후변화 감시, 해양영토관리를 위한 과학적 근거 자료 확보 **(생태적/기후적 건강성 평가 및 지수 산출)** 및 자원으로서의 가치 창출

□ 남해역 무인도서의 통합적 관리 방안 수립 및 자원 가치 창출

□ 남해역 최외곽 및 전략 (무인)도서 및 주변 해역에 대한 체계적이고 종합적인 해양과학 조사를 통한 해양환경 보전, 기후변화 감시, 해양영토관리를 위한 과학적 근거 자료 확보

○ 전지구적 해양환경 변화 감시를 위한 표준정점 설정과 중장기적 모니터링을 통한 고감도 생물지시자 개발과 기후/환경변화 연구

○ 기후 변동에 따른 각 무인도서 해역 간의 수서 생태계 먹이망 구조 및 기능 변화 예측 기술 개발

○ 영토관리를 위한 해양과학적(위치, 영해기점, 명칭 등)-인문사회학적(무인도서의 역사적 가치 등) 자료 구축 및 국가정책 확보

○ 남해역의 생태적/기후적 건강성 평가 및 지수 산출

□ 남해역 무인도서의 통합적 관리 방안 수립 및 자원 가치 창출

○ 최외곽 (무인)도서와 주변 해역에 대한 해양환경/생태 특성 파악 및 생태축으로서의 역할 규명하고, 다양한 자원으로서의 가치 평가

○ 도서 주변 해양환경의 인문사회과학-해양과학적 종합 정보도 작성과 이에 근거한 보존무인도서, 이용가능무인도서, 개발가능무인도서 등 보전과 개발을 위한 관리체계를 구축하고 해양생태계보전도서, 해양경관보전도서, 해양생물보전도서 등의 해양보호구역 설정을 위한 정책자료 도출

2. 국내외 연구개발 동향·분석

2.1. 관련 연구/기술의 국내외 동향

국외 동향

○ 국외 여러 국가에서 도서와 주변 해양의 환경과 생태계를 보호하고, 해양영토의 기준점을 확보하고 더 나아가 관광자원으로써의 개발을 위해 전략적으로 관리하고 모니터링하고 있음.

○ 미국의 경우에는 해양생태계를 보호할 목적으로 도서와 주변 해양을 관리를 하고 있으며, 크게 하와이 생태계보전지역 관리체제와 산호초관리단 운영 정책으로 나눌 수 있음(해양수산부, 2005). 특히 하와이 군도 산호초 생태계 보호를 위해 대통령령을 통해 종합적인 관리체제 구축하고 있음.

○ 중국의 경우 2001년 6,100개가 넘는 중국의 무인도서 보호 및 관리를 위한 지침을 발표함. 면적이 500m2 이상인 섬은 6,500개로 이중 433개가 유인도서이며, 모든 무인도서에 이름을 부여하고, 특별한 가치가 있는 무인도서의 경우 보호지역으로 지정할 것을 제시하고 있음. 특히 해양영토 기점으로서 무인도서의 중요성과 이에 대한 체계적 관리의 필요성을 인식하고 무인해도의 보호 및 이용에 관한 관리 규정을 2003년에 마련함. 무인도서와 구별되는 무인해도는 통상적 의미의 무인도서 뿐만아니라 암초, 저조고지(수중 고지대)를 모두 포함함. 이러한 포괄적 개념의 무인해도는 일반적인 해양환경과 생태계보전 측면 뿐만아니라 영토분쟁과 관련한 중국의 정책을 반영한 결과로 해석됨. 또한 중국의 무인해도 관리제도는 도서의 관리 범위를 육지부에 한정하지 않고 해면부까지 확장하고 있어 공간통합관리를 강조하고 있으며, 영해의 기점이 되는 무인해도에 대해서는 엄격한 보호제도를 실시하고 있음. 즉, 영해기점에 소재하는 무인해도와 주변 해역에 대해서는 파괴성 활동을 금지하고 있음. (해양수산부, 2005)

○ 몰디브는 약 200개의 유인도서와 약 1,000개의 무인도서로 이루어져 있으며, 주로 생태적, 관광적 가치를 활용할 목적으로 무인도서를 관리 개발하고 있음. 몰디브 관광산업(전체 GDP의 약 33%)을 위한 모든 리조트 건설은 무인도서로 제한되어 있으며, 엄격한 환경기준이 적용됨 (해양수산부, 2005).

국내 동향

○ 국내에서는 환경부의 “독도등도서지역의생태계보전에관한특별법” 제정을 계기로 전국무인도서 자연환경조사를 1998년부터 시작함. 해양수산부 또한 “무인도서의보전및관리”에 관한 법률을 제정하고 2005년에 일부 무인도서 실태조사를 실시함.

○ 환경부는 전국무인도서 자연환경조사를 통하여 1998년부터 2006년까지 총 708개의 무인도서 실태 조사를 실시하였으며, 이중 153개를 특정도서로 지정하여 보전-관리하고 있음. 그러나 무인도서 주변해역의 해양생태계는 육지에 가까운 연안해역의 생태계와는 기능과 구조가 다른 보전가치가 높은 환경임에도 불구하고 기존에 시행된 무인도서 자연환경조사는 도서의 육상생태계에만 초점이 맞추어짐. 따라서 생물 다양성이 매우 높고, 건강한 환경/생태계를 유지하고 있는 무인도서 주변 해양생태계를 조사할 필요성이 있음.

○ 결론적으로 미국, 중국 등 외국의 경우 무인도서를 도서에 국한하여 관리하는 것이 아니라 육지부와 해면부(주변 해양)를 통합한 하나의 생태단위 또는 자원단위로 인식하고 관리함. 즉, 무인도서 관리에서 육지부와 해면부 사이의 에너지 교환, 생태적 연결성을 고려하지 않고서는 지속 가능한 발전, 합리적인 이용, 체계적인 보전에 한계가 있음. 또한 우리의 주변국인 중국의 경우 무인도서를 영해 기점 도서로서 전략적으로 관리하고 있음. 그러나 우리의 기존 연구는 대부분 육지부에 국한되어 조사 되었으며, 더욱이 각 무인도서가 갖는 독특한 해양생태계에 대한 특성 규명, 이들 생태계 사이의 연결 고리, 그리고 연안역 미치는 영향 등은 연구되지 않음. 특히 영해의 기선이되는 도서 그리고 최외곽의 도서들에 대해서는 시급한 조사와 통합적 관리가 필요함.

2.2. 관련기술의 시장규모 및 적용가능 분야

가. 관련기술의 시장규모

◇ 본 연구는 기술개발 관련 사업이 아님. 그러나 무인도서에 대한 해양관광자원으로서의 가치 창출은 향후 국민 복지와 관련 해양조선 산업에 큰 파급효과가 있을 것으로 기대됨

나. 관련기술의 적용가능 분야

기술분류	적용 가능 분야
	○ 해양환경 보존 및 보전 기술 ○ 기후변화 감시 기술 ○ 해양경계획정 전략 방안 기술

3. 연구개발 목표

□ 최외곽 및 전략 (무인)도서 및 주변 해양 환경/생태계 특성 규명 및 생태축 연구

□ 기후변화 연구 및 영토관리를 위한 해양과학적 근거 자료 (해양생태적/기후적 건강성 평가 및 지수 산출) 확보

□ 남해역 무인도서와 주변 해양환경 보전/개발을 위한 체계적 통합적 관리 방안 도출

□ 해양관광자원으로 가치 창출

3.1. 최종목표

□ 국가적 현안인 문제(해양환경 보전, 기후변화와 영토관리) 해결을 위한 남해역 최외곽 및 전략 (무인)도서 주변에서의 해양과학적 근거 자료 (해양생태적/기후적 건강성 평가 및 지수 산출) 도출 및 무인도서 관리방안 수립

3.2. 단계별 연구 목표

□ 제1단계(2009~2011년): 남해역 소권역* 무인도서 및 주변 해양 환경/생태 특성 규명 및 환경/생태/기후 변화 모니터링

*남해역에 위치하고 있는 무인도서를 연안 및 외해 해양환경을 고려하여 3개의 소권역으로 나누어, 권역별로 무인도서중 가장 외해쪽에 위치한 무인도서부터 환경/생태 특성 조사함. 또한 중요 무인도서 주변 해역에서 외래 생물 유입 등의 환경/생태 변화 및 기후변화 모니터링.

□ 제2단계(2012~2014년): 제1단계에서 확보된 연구기반을 근거로 2단계 소권역 무인도서의 환경/생태계 특성을 파악 (계속) 및 생태축 규명. 중요 무인도서 주변 해역에서 외래 생물 유입 등의 환경/생태 변화 및 기후변화 모니터링(계속). 중요 무인도서에 대한 관리 방안 도출.

□ 제3단계(2015~2017년): 3단계 권역 무인도서 조사(계속). 1단계와 2단계에서 도출된 자료를 토대로 각 무인도서별 특성을 구분하고, 무인도서간 생태축 정보도 작성. 남해역의 기후변화 및 환경 변화 연구. 생태계보전과 영토관리를 위한 남해역 무인도서 종합적 관리 방안 도출 및 국가적 중요 무인도서 보전/개발 방향 도출

4. 연구내용 및 범위

4.1. 연구목표 및 범위

목표	연구내용	연구범위
최외곽 무인도서 및 주변 해양환경/생태계의 보전과 국가적 현안인 문제(기후변화와 영토관리) 해결을 위한 무인도서 관리방안 연구	무인도서 및 주변 해양 환경/생태계 특성 규명 및 생태축 연구	- 해양지질환경(무인도서 위치, 면적, 해안선 길이, 육지와의 거리, 근접도서거리, 지질-지형, 경관, 해저 지형 등) 특성 규명 - 무인도서와 주변(만조선으로부터 약 1km) 암반/수중/해저의 정밀 해양생태환경 특성 규명 및 생물종 다양성 조사 - 무인도서 주변 해양생태계 건강성 평가 - 무인도서 주변 보호 생물종/해조군락 조사 - 무인도서들 사이의 환경/생태학적 연관성 조사
	기후변화 연구 및 영토관리를 위한 해양과학적 근거자료 확보	- 전지구적 해양환경 변화 감시를 위한 외래 유입종 모니터링 및 고감도 기후변화 지시종 개발을 통한 해양환경 및 기후변화 연구 (남해역 기후변화 감시를 위한 고감도 생물지시자 개발 및 활용방안 연구) - 기후 변동에 따른 각 해역 간의 수서 생태계 먹이망 구조 및 기능 변화 연구
		- 무인도서의 주변 해역(무인도서의 육지부와 이에 연결된 해양생태계의 영향한계 범위) 범위 설정(현재는 과학적 근거 자료가 없어 골재채취법의 골재채취 한계범위를 준용하여 도서의 크기, 면적, 생태계 특성과 관계없이 1km로 설정함.) - 영토관리를 위한 기선기준점 검토 (무인도서 위치, 영해 기점, 도서명칭 등) - 해양경계 주변해역에서의 새로운 무인도서(또는 암초) 탐색 - 무인도서 공간자료 확보 (항공사진, 수치지형도, 수치해도, 위성영상 등)
	무인도서와 주변 해양환경 보존/개발을 위한 정책적 관리 방안 도출	- 무인도서의 생태학적(생태축)/생물학적(생물자원)/관광자원학적(주변환경, 관광객 방문)/사회과학적(무인도서의 역사적 가치) 가치 평가 - 무인도서 인문사회과학-해양과학적 종합 정보도 작성 - 무인도서 보존/개발을 위한 유형(또는 특성)별 전략적 관리 방안 도출 예) 무인도서의 종합 정보에 근거한 보존무인도서, 이용가능무인도서, 개발가능무인도서 등 보전과 개발을 위한 관리체계를 구축하고 해양생태계보전도서, 해양경관보전도서, 해양생물보전도서 등의 해양보호구역 설정을 위한 자료 도출

4.2. 연구대상기술의 개발 가능성

◇ 무인도서 및 주변 해양 환경/생태계 특성 규명 및 생태축 연구

- ○ 구무인도서 및 주변 해양환경/생태계 특성 규명 및 생태축 연구는 현재 남해특성연구부에 구축된 인력 풀로 충분히 목표달성 가능
- ○ 기존의 무인도서자연환경조사 사업의 결과 및 남해역 환경/생태조사 사업들의 결과들을 함께 활용하여 남해역과 무인도서의 환경/생태 상관성을 파악하여 생태축 연구 가능

◇ 기후변화 연구 및 영토관리를 위한 해양과학적 근거 자료 확보

- ○ 국내 전국 연안 (약 100개 정점에서 총 시료 약 1,000개)에서 조사된 원생생물 종류의 출현양상을 파악하고 해역별 지시종 탐색을 통한 정밀 기후변화 탐색 가능
- ○ 매우 중요한 전략적 가치가 있는 최외곽 무인도서 및 수중 암초에 대한 정밀 해양과학조사를 통한 기선기준점 재검토 (중국의 경우 양쯔강 하구에서 동쪽 69해리 떨어진 무인암석 해초를 EEZ 기점으로 정함.)

◇ 무인도서와 주변 해양환경 보존/개발을 위한 정책적 관리 방안 도출

- ○ 무인도서에 대한 인문사회-해양과학적 자료를 바탕으로 기존연구에서 제시된 관리문제점과 관리실태, 최근의 정책수요를 현재의 관리체제가 충족할 수 있는지 여부를 종합함으로써 통합적 관리체제 방안 도출 가능

4.3. 단계별 수행 연구개발 과제

□ 제1단계(2010~2012년)

- ○ 최외곽 및 전략 무인도서 및 주변 해역의 해양환경/생태 특성 규명
- ○ 해양환경 및 기후변화 민감 생물종 연구 및 모니터링

□ 제2단계(2013～2015년)

○ 무인도서 및 주변 해역의 해양환경/생태 특성 규명(계속)

○ 환경 및 기후변화 민감 생물종 연구 및 모니터링(계속)

○ 남해역과 무인도서의 환경/생태 상관성 파악 및 생태축 연구

○ 국가적 중요 무인도서 보전/개발 방향 도출

□ 제3단계(2016～2018년)

○ 무인도서 인문사회-해양과학적 정보도 작성.

○ 남해역의 기후변화 및 환경 변화 연구
(생태적/기후적 건강성 평가 및 지수 산출)

○ 생태계보전과 영토관리를 위한 남해역 무인도서의 유형별(또는 특성별) 종합적 관리 방안 도출

4.4. 기술개발 및 시장점유 가능성

- 해당사항 없음

5. 연구개발 추진전략 및 체계

5.1. 기본방안

◇ **연구목표 및 성과의 정량화**
- 최외곽 및 전략 무인도서 및 주변 해양환경/생태계의 특성 규명에 의한 환경적/기후적 건강성 평가 및 지수 산출 (정량화)
- 연구결과의 검증을 위한 논문 발표

◇ **국내 산·학·연·관 연구역량을 결집**
- 대학, 연구기관, 정부부처 등을 포괄하는 연구 체제 구축
- 기존 "전국무인도서자연환경조사"팀과의 유기적 관계 구축 및 통합 자료 구축

◇ **무인도서 해양과학적 자료 확보 및 정책 방안 도출 을 통한 국가적 현안 문제 해결을 위한 연구결과 즉각적 활용**
- 남해역 무인도서의 유형별 또는 그룹별 관리 방안 제시

5.2. 추진전략

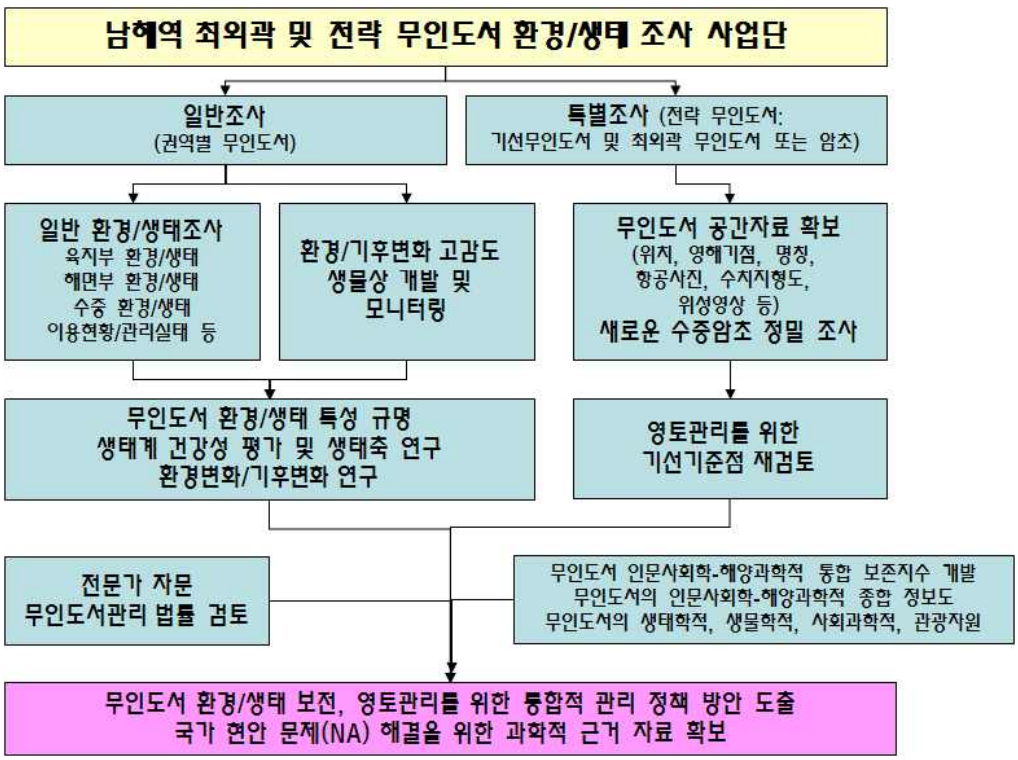

5.3. 연구개발 추진일정

분류	핵심기술 연구내용	1단계			2단계			3단계			비고
		10	11	12	13	14	15	16	17	18	
	- 최외곽 및 전략 무인도서 및 주변 해역의 해양환경/생태 특성 규명 - 해양환경 및 기후변화 민감 생물종 연구 및 모니터링	■	■	■							
	- 무인도서 및 주변 해역의 해양환경/생태 특성 규명(계속) - 환경 및 기후변화 민감 생물종 연구 및 모니터링(계속) - 남해역과 무인도서의 환경/생태 상관성 파악 및 생태축 연구 - 국가적 중요 무인도서 보전/개발 방향 도출				■	■	■				
	- 무인도서 인문사회-해양과학적 정보도 작성. - 남해역의 기후변화 및 환경 변화 연구 - 생태계보전과 영토관리를 위한 남해역 무인도서의 유형별(또는 특성별) 종합적 관리 방안 도출							■	■	■	

6. 기대성과 및 활용방안

○ 해양생태계의 박물관인 무인도서와 주변 해양 환령/생태계 보전 및 도서지역의 새로운 독특한 해양생물자원 확보와 생명공학 산업에의 활용

○ 생물상이 우수하고 생태적, 자원학적, 관광적 측면에서 가치 있는 무인도서의 보전 정책 유도

○ 영해기점 및 최외곽 도서 등에 대한 종합적 해양과학 조사를 통한 영토주권 및 생물자원 주권 확보

○ 기후/환경문제는 더 이상 국내만의 문제가 아니며, 국제적으로 논의될 수 있는 다양한 방안에 대해 대처할 수 있는 독자적인 체제 구축 가능

7. 결론 및 정책적 시사점

7.1. 결론

결 론

▶ 남해역의 무인도서 주변 해역은 상대적으로 인간의 간섭이 적어 생물학적, 환경학적, 생태학적, 해양자원 및 관광학적 가치가 매우 높고, 도서마다의 독특하고 고유한 지형/지질/환경/생태 특성을 유지하고 있어 보전/관리 방안이 필요함.

▶ 또한 따라서 국가적 현안인 문제(해양환경 보전, 기후변화와 영토관리) 해결을 위한 남해역 최외곽 및 전략 (무인)도서 주변에서의 해양과학적 근거자료 (해양생태적/기후적 건강성 평가 및 지수 산출) 도출 및 무인도서 관리방안 수립이 필요함.

▶ 본 연구는 무인도서의 보전 및 관리에 관한 법률에 근거하고 있으며, 국가적 현안(NA)인 환경보전, 기후변화, 영토관리에 관한 해양과학적 근거자료를 도출하는 연구임.

▶ 남해는 다도해로 약 2,034개의 무인도서가 존재하며, 이들 중 최외곽 및 전략적 (무인)도서가 갖는 가치는 매우 중요하다고 판단되며, 이러한 무인도서의 범국민적 이용과 가치 창출을 위해서는 국가적인 차원의 무인도서의 해양과학 조사 프로그램 마련이 시급함.

7.2. 정책적 시사점

정책적 시사점

▶ 본 연구를 통하여 무인도서와 주변 해양환경/생태계에 대한 과학적 근거 자료를 확보함으로써 국가적으로 시급히 해결해야할 해양영토관리, 기후변화, 해양환경보전 등에 대한 정책적 대응방안 수립이 가능함.

▶ 남해는 다도해로 약 2,034개의 무인도서가 존재하며, 이들이 갖는 관광자원으로서의 가치는 무한하며, 향후 녹색성장과 함께 국민의 복지 증진과도 밀접한 관련이 있음.

8. 소요예산

□ 총 연구비 : 270억(90억/년)

(단위 : 억원)

연구 분야	1단계			2단계			3단계			합 계
	'10	'11	'12	'13	'14	'15	'16	'17	'18	
무인도서 및 주변 해양환경/생태계 특성 규명 및 생태축 연구	15	15	15	15	15	15	15	15	15	135
기후변화 연구 및 영토관리를 위한 해양과학적 근거 자료 확보	10	10	10	10	10	10	10	10	10	90
무인도서와 주변 해양환경 보존/개발을 위한 정책적 관리 방안 도출	5	5	5	5	5	5	5	5	5	45
총 액										270

연구과제제안요구서(RFP)

과 제 명	남해역 최외곽 및 전략 (무인)도서 주변 해양과학 조사와 통합적 관리 방안 수립
연구의 필요성	○ 남해의 무인도서 주변 해역은 상대적으로 인간의 간섭이 적어 생물학적, 환경학적, 생태학적, 해양자원 및 관광학적 가치가 매우 높고, 도서마다의 독특하고 고유한 지형/지질/환경/생태 특성을 유지하고 있어 생태계의 박물관(생태축)으로서 보존가치가 매우 큼 ○ 도서(섬)는 실효적 지배와 이용정도에 따라 중요한 영토학장 즉 해양 경계획정의 기준이 되는 기선 기준점(영해기점 무인도서)임. ○ 그러나 무인도서와 주변 해양환경/생태 보존, 보전, 개발을 위한 체계적, 종합적 해양과학 조사 및 연구 자료가 부족하며, 특히 영토관리를 위한 영해 기점도서 및 최외곽 도서/암초에 대한 정보 또한 부족함. ○ 따라서 해양영토관리, 기후변화, 해양환경보전 등의 국가적 현안을 해결하기 위한 무인도서와 주변 해양에 대한 종합적 관리가 필요함.
연구의 목적	○ 남해역 최외곽 및 전략 (무인)도서 주변 해양에 대한 체계적이고 종합적인 해양과학 조사를 통한 해양환경 보전, 기후변화 감시, 해양영토관리를 위한 과학적 근거(해양생태적/기후적 건강성 평가 및 지수 산출)자료 확보 ○ 남해역 무인도서 통합적 관리 방안 수립 및 가치 창출
연구 내용 및 범위	○ 무인도서 및 주변 해양 환경/생태계 특성 규명 및 생태축 연구 - 무인도서와 주변의 해양지질환경 특성 규명 - 암반/수중/해저의 정밀 해양생태환경 특성 규명 및 생물종 다양성 조사 - 무인도서 주변 보호 생물종/해조군락 조사 및 해양생태계 건강성 평가 - 무인도서들 사이의 환경/생태학적 연관성 조사 ○ 기후변화 연구 및 영토관리를 위한 해양과학적 근거 자료 확보 - 지구적 해양환경 변화 감시를 위한 외래 유입종 모니터링 및 고감도 기후변화 지시종 개발을 통한 해양환경 및 기후변화 연구 - 영토관리를 위한 기선기준점 검토 (무인도서 위치, 영해 기점, 도서명칭 등) - 해양경계 주변해역에서 새로운 무인도서(또는 암초) 탐색 및 공간자료 확보 ○ 무인도서와 주변 해양환경 보존/개발을 위한 정책적 관리 방안 도출 - 무인도서 인문사회과학-해양과학적 종합 정보도 작성 - 무인도서 보존/개발을 위한 유형(또는 특성)별 전략적 관리 방안 수립
추진방법	○ 국내외 전문가를 중심으로 working group을 구성・운영 ○ 환경부에 수행한 "전국무인도서자연환경조사" 및 국토해양부에서 수행중인 "해양생태계기본조사" 결과 활용
연구비/년	○ 1년차 (90억/3년) ○ 2년차 (90억/3년) ○ 3년차 (90억/3년)
연구 성과물	○무인도서 및 주변 해역의 인문사회-해양과학적 정보도 ○무인도서 및 주변 해역의 유형/특성별, 보존/개발 통합 관리방안 정책 ○국가 현안 문제인 기후변화, 영토확장 등의 과학적 근거 자료 확보 ○과학적 국내외 논문

Chapter Ⅱ. 연구논문 성과

1) Methane-derived authigenic carbonates from the Ulleung basin sediments, East Sea of Korea. Continental Shelf Research, 29 (2009) 1588-1596. 임동일, 최진용, Z. Xu, 김문구, 최동림, 정회수, 이판묵

2) Rare Earth elements in the bottom sediments of major rivers around the Yellow Sea: implications for sediment provenance. Geo-Maarine Letters, in press (2009). Z. Xu, 임동일(교신저자), 최진용, 양수업, 정회수

3) Sea-cliff erosion and retreat in semi-enclosed macrotidal embayment: Hampyung Bay, west coast of Korea. J. Coastal Research, SI 56 (2009) 732-736. 임동일, 최진용, 정회수

Continental Shelf Research 29 (2009) 1588–1596

Contents lists available at ScienceDirect

Continental Shelf Research

journal homepage: www.elsevier.com/locate/csr

Methane-derived authigenic carbonates from the Ulleung basin sediments, East Sea of Korea

Dhongil Lim [a,*], Jinyong Choi [b], Zhaokai Xu [b,c], Moonkoo Kim [a], Donglim Choi [a], Hoisoo Jung [d], Panmook Lee [e]

[a] South Sea Institute, Korea Ocean Research and Development Institute, 391 Jangmok-ri Jangmok-myun Geoje 656-830, Republic of Korea
[b] Department of Oceanography, Kunsan National University, Kunsan 573-701, Republic of Korea
[c] Key Laboratory of Marine Geology and Environment, Institute of Oceanology, Chinese Academy of Sciences, Qingdao 266071, China
[d] Marine Geoenvironment and Resources Research Division, Korea Ocean Research and Development Institute, Ansan, P.O. Box 29, Seoul 425-600, Republic of Korea
[e] Marine and Ocean Engineering Research Institute, Korea Ocean Research and Development Institute, 171 Jang-dong Yuseong, Daejeon 305-343, Republic of Korea

ARTICLE INFO

Article history:
Received 3 November 2008
Received in revised form
22 April 2009
Accepted 30 April 2009
Available online 18 May 2009

Keywords:
Authigenic carbonates
Methane seep environments
Gas hydrate
East Sea (Japan Sea)

ABSTRACT

Authigenic carbonates were sampled in methane-enriched piston core sediments collected from gas venting sites on the western continental slope of the Ulleung Basin, East Sea of Korea. Multidisciplinary investigations on these carbonates, including the scanning electronic microscope (SEM) observations and mineralogical-geochemical compositions, were carried out to identify the carbon and oxygen sources and the forming mechanism of these carbonates. The authigenic carbonates from the study area correspond to semi-consolidated, compact concretions or nodules ranging from 2 to 9 cm in size. X-ray diffraction and electron microprobe analyses showed that most of the sampled carbonate concretions were composed of almost purely authigenic high-Mg calcite (10.7–14.3 mol% $MgCO_3$). Characteristically, microbial structures such as filaments and rods, which were probably associated with the authigenic minerals, were abundantly observed within the carbonate matrix. The carbonates were strongly depleted in $\delta^{13}C$ (−33.85‰ to −39.53‰ Peedee Belemnite (PDB)) and were enriched in $\delta^{18}O$ (5.16–5.60‰ PDB), indicating that the primary source of carbon is mainly derived from the anaerobic oxidation of methane. Such methane probably originated from the destabilization of the underlying gas hydrates as strongly supporting from the enriched ^{18}O levels. Furthermore, the strongly depleted $\delta^{13}C$ values (−60.7‰ to −61.6‰ PDB) of the sediment void gases demonstrate that the majority of the gas venting at the Ulleung Basin is microbial methane by CO_2 reduction. This study provides another example for the formation mechanism of methane-derived authigenic carbonates associated with gas-hydrate decomposition in gas-seeping pockmark environments.

1. Introduction

The East Sea is a mid-latitude, semi-enclosed deep marginal sea (average water depth of 1350 m) surrounded by Korea, Japan, and Russia (Fig. 1). Structurally, it comprises three basins (the Ulleung Basin, the Japan Basin, and the Yamato Basin), which are separated by the Korea Plateau, Oki Bank, and Yamato and Kita-Yamato Ridges. The East Sea, especially Ulleung Basin is a region where well-developed gas seepage-related structures are widely distributed in deep-water environments (Gardner et al., 1998; Horozal et al., 2009). Acoustic backscatter imagery data obtained in this basin showed well-developed seepage-related structures, which are interpreted to be pockmarks, or mounds likely created by seepage of methane (CH_4)-rich fluids (Gardner et al., 1998). Recently, multi-channel seismic investigation in the Ulleung Basin, East Sea, showed various seismic indicators of the presence of gas hydrate and associated gas, including the bottom-simulating reflector (BSR), and seismic chimneys (Horozal et al., 2009). The presence of both BSR and pockmarks suggested that the East Sea must be an active gas-seeping region, comparable to the Black Sea, which is the world's largest anoxic marine basin (Mazzini et al., 2004). In addition, occurrence of carbonate ($CaCO_3$) nodules from the piston core sediments from the Ulleung Basin of the East Sea was reported (Dr. D. Yoo, personal communication).

At the active fluid seepage areas, precipitation of authigenic carbonate is a common phenomenon, which is related to the activity of archaea and bacteria oxidizing methane near the seafloor (Ritger et al., 1987; Boetius et al., 2000). Accordingly, authigenic carbonate precipitation in cold seep environments is one of the most important indicators for the presence of gas-rich fluids, which may indicate, in some cases, presence of shallow gas hydrates (e.g., Ritger et al., 1987; Bohrmann et al., 1998; Aloisi

* Corresponding author. Fax: +82 55 639 8589.
E-mail address: oceanlim@kordi.re.kr (D. Lim).

0278-4343/$ - see front matter © 2009 Elsevier Ltd. All rights reserved.
doi:10.1016/j.csr.2009.04.013

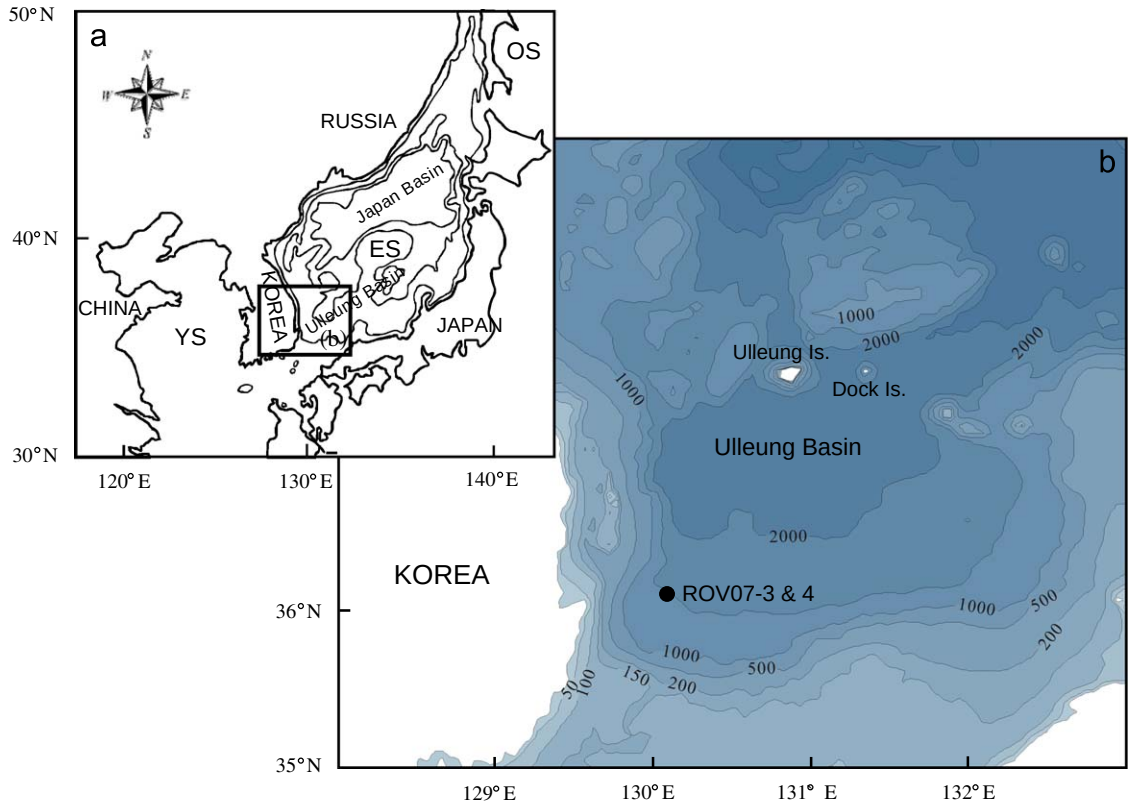

Fig. 1. Map showing (a) study area and (b) core location in the study area with bathymetry (m). ES: East Sea, YS: Yellow Sea, and OS: Okhotsk Sea.

et al., 2000; Greinert et al., 2001; Luff and Wallmann, 2003; Lu et al., 2005; Chen et al., 2006; Bayon et al., 2007). The typical seep carbonate mineral species are mainly composed of microcrystalline calcite, aragonite, and dolomite (Peckmann et al., 2001; Lu et al., 2005; Chen et al., 2006), although the chemo-physical factors controlling the mineralogy of seep carbonates are still incompletely understood. Recent studies have shown that authigenic carbonate can occur as discrete phases throughout the sediment column at cold seeps, with a wide variety of lithologies and carbonate compositions, in relation to the presence of gas hydrate (Rodriguez et al., 2000; Bayon et al., 2007). The identification of such carbonate phases in marine sediments can therefore provide a unique window into the distribution and magnitude of ancient seep settings.

Here, we present internal micro-texture, and geochemical and mineralogical data for authigenic carbonates recovered from gas hydrate-bearing sediments in the Ulleung Basin of the East Sea and further focus on the relationship between these carbonates and the gas hydrate, especially the origin of the fluids and the possible evidence of gas hydrate dissociation.

2. Materials and methods

Two piston cores (ROV07-3 and 4) were taken from the western slope region (approximately 1500 m water depth) of the Ulleung Basin, East Sea, where gas-seeping structures were observed. The cores, with lengths of 1.8 and 3.2 m, were split lengthwise, photographed, and logged in detail by visual examination. Grain-size analysis was carried out by a standard dry-sieving technique for the sand fraction ($>4\varphi$) and by a pipette method for the mud fraction ($<4\varphi$). Total carbon (TC) and organic carbon (OC) contents of the sediments (dry wt%) were determined using a Carlo Erba Elemental Analyzer 1108 (CE Instruments, Milan, Italy), the carbonate content being calculated using the equation $CaCO3\ (\%) = (TC–OC) \times 8.333$ (Stein et al., 1994).

Sediment samples for pore water CH_4 analysis were collected using a tipless syringe from pre-drilled holes on plastic liner of cores and then transferred into 50 mL gas-tight serum vials containing 20 mL NaOH solution (Ferdelman et al., 1997). Methane concentrations of the samples were determined by injecting an aliquot of headspace into a gas chromatograph coupled with indium oxide (InO_2) semiconductor detector (GC/SCD, Sensortec GS-23, Japan). The separation of gases was accomplished by the column (stainless steel, 2 m × 3 mm i.d.) packed with molecular sieve (13X-S, 60/80 mesh, GL Science Co., Japan). Details on the methane analysis using GC/SCD are given in Ohta et al. (1999).

The stable carbon isotope ratios of methane in sediment void gas and gas hydrates were measured in the geochemistry laboratory at the Hokkaido University (Japan) by the method of Tsunogai et al. (2002). Briefly, an aliquot of hydrate-bound and/or void gases was injected into a gas chromatograph and methane was separated from gas mixture by a 25 m long, 32 μm i.d., PoraPLOT-Q capillary column. Separated methane was then quantitatively combusted to CO_2 and the isotopic composition of CO_2 gas was measured using a mass spectrometer (Finnigan MAT 252). Stable carbon isotope ratios are reported in the standard δ-notation in per mil (‰) relative to Peedee Belemnite (PDB) standard and the precision of the analysis was estimated to be 0.3‰.

For this study, carbonate concretions were collected at various depths (4–6, 9–11, 20–21.5, 28, 31–32.5, 41–42.5, and 237 cm) along the ROV07-4 core. Bulk mineralogy was determined on compressed powder pellets using a high quality XG X-ray diffractometer (XRD) with Cuk_α radiation. XRD patterns were obtained from 3° to 47° 2θ at a scanning speed of 0.04° 2θ/s at conditions of 40 kV and 40 mA. The microstructure on fresh surfaces and thin sections of selected carbonate concretion

samples was examined by scanning electronic microprobe (SEM, Model: Hitachi S-4800). The chemical composition of selected mineral phases was also assessed by energy dispersive spectroscopy (EDS). Stable carbon and oxygen isotope measurements on bulk concretions were performed by liberating CO_2 via the standard phosphoric acid technique (McCrea, 1950; Sharma and Clayton, 1965) in Korea Basic Science Institute, Korea (KBSI). Measurements were made with a carbonate preparation system linked with a mass spectrometer. The $\delta^{13}C$ and $\delta^{18}O$ results are given relative to the PDB reference, with a precision of 0.2‰ for both isotope composition values.

3. Results

3.1. General description of sediment cores

Cores from the gas-seeping area of the Ulleung Basin are composed mainly of stiff, dark-to-olive grayish (5Y 4/1 or 5Y 4/2) silty clay (>50% in clay content) sediments, which are largely disturbed with many cracks (Fig. 2a). These cracks are considered to be degassing structures, which may be produced by expansion of gas due to decompression and temperature rise. The sediments range from 5.3φ to 9.0φ in mean grain size, and physical sedimentary structure is not observed. Calcium carbonate contents in sediments accounted for between 13 and 47 wt% of the sediments, and organic carbon contents ranged from 1.4% to 3.8%. The sediment core exhibited significant enrichment in dissolved methane. In core ROV07-4, methane was highly saturated even at 30 cm depth (ca. 260 μmol/L; Fig. 2b), with concentration increasing significantly with depth (up to 8000 μmol/L at 300 cm depth). In addition, these sediments contained abundant carbonate concretions (Fig. 2a, see description below). A gas hydrate layer was also present at the base of core ROV07-4.

3.2. Morphology, mineralogy, and isotopic compositions of carbonate concretions

In the studied cores, most of carbonate concretions occurred just below the seafloor or in shallow sediments. These carbonates correspond to mostly grayish, roughly spherical bodies ranging from 2 to 9 cm in diameter (Fig. 3). Most carbonate samples from this region were compact concentrations in appearance, frequently with a slightly loose, porous surface. These compact concretionary samples clearly differed from the authigenic carbonate nodules and/or slabs with holes and porous surfaces found in the nearby South China Sea and Okhotsk Sea (Greinert et al., 2002; Lu et al., 2005; Chen et al., 2006; Han et al., 2008).

SEM observations with EDS analysis revealed that carbonate concretions were characterized by a compact (Fig. 4a), and were mainly composed of pure calcite, together with other minor carbonate minerals (aragonite and siderite) and abundant biological impurities. Calcite consistently appeared in roughly equigranular, anhedral crystals of about 5 μm in size (Fig. 4b). Aragonite was observed occasionally in only one sample from core ROV07-4, at ~32 cm depth, occurring as large radiating elongated crystals (Fig. 4c). In addition, agglomerates of euhedral siderite rhombs were observed in some samples (Fig. 5). The size of individual siderite rhomb was about 1 μm, while their agglomerates were spherical in shape and several microns in size. Siderite usually appeared within cavities formed by biological fragments. Abundant microbiological (e.g., diatoms, worm tubes) and microbiological (e.g., biofilms, filaments) materials were also observed under SEM, especially in the

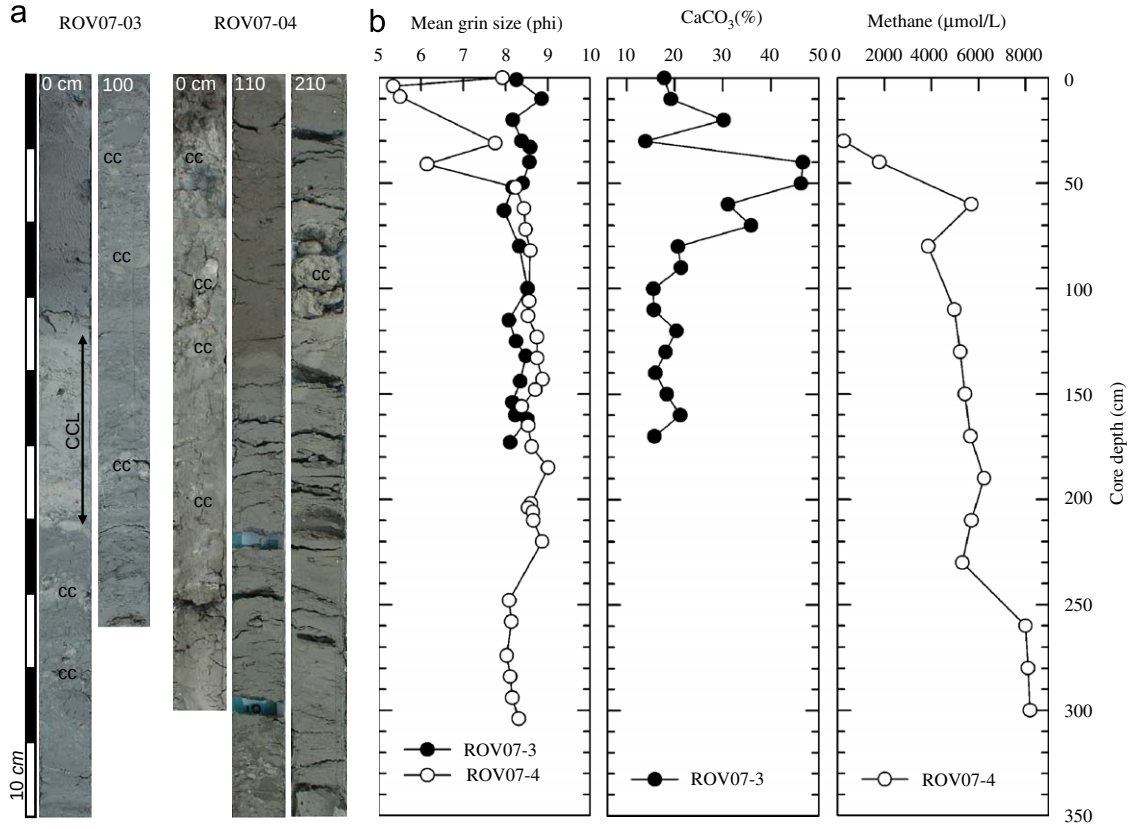

Fig. 2. (a) Photographs of core sections with abundant authigenic carbonate concretions (cc) and multiple cracks generated by gas expansion and (b) vertical profiles of mean grain-size, $CaCO_3$ contents and methane concentrations in ROV07-03 and/or 04 sediments.

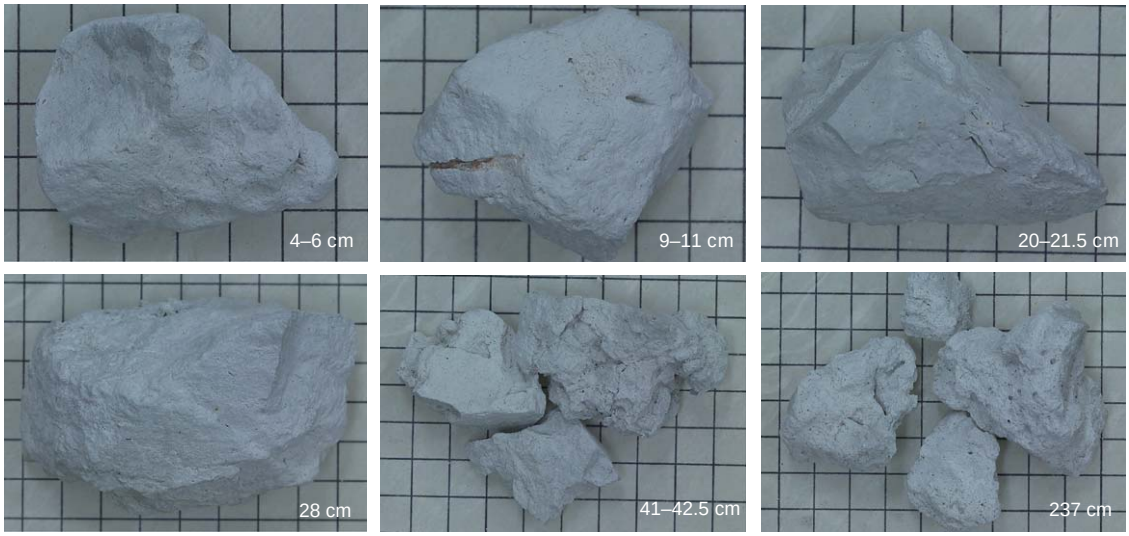

Fig. 3. Authigenic carbonate concretion samples recovered in different depths of core ROV07-4. Note most of them, except for the ones at 237 cm, appear in the form of compact lump without porous surface, obviously different to the previously reported ones with porous surface in nearby seas. Scale bar is 2 cm.

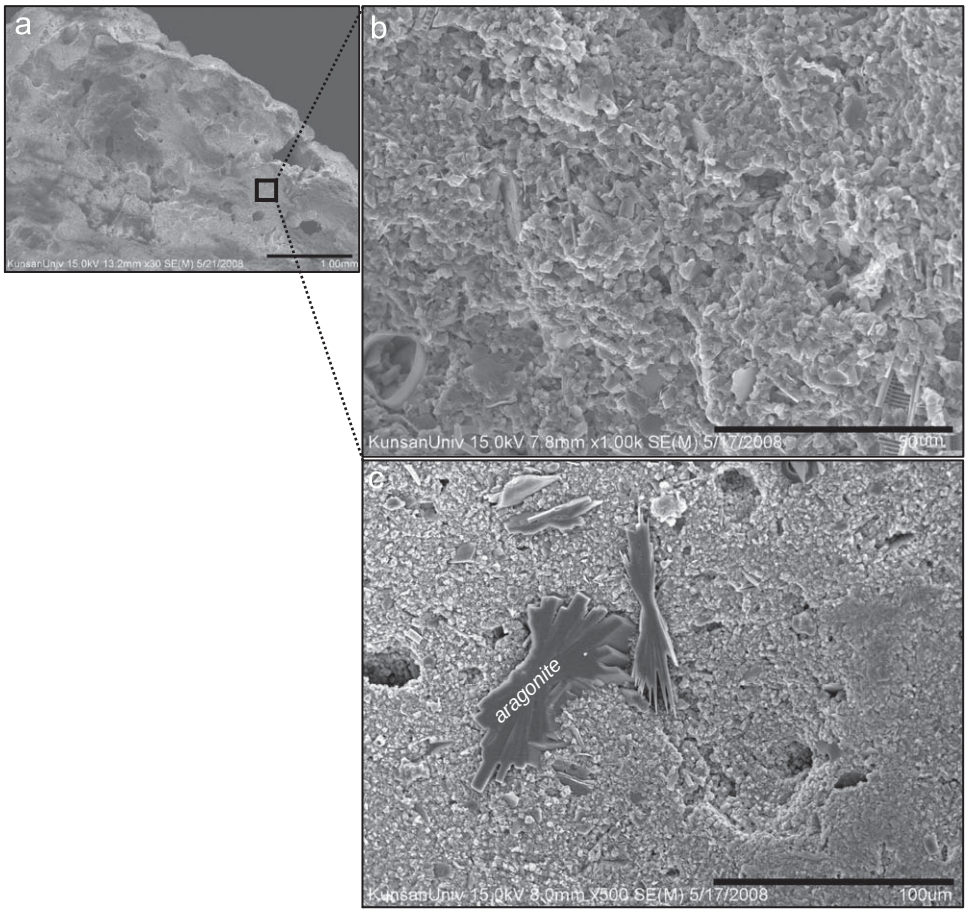

Fig. 4. SEM photographs showing (a) the compact and rough surface of authigenic carbonate, (b) the roughly equigranular, anhedral calcite crystals and various biological impurities, and (c) the elongated aragonite crystals.

carbonate samples from the lower section of the core (Fig. 6). The microbial filaments from this study are similar in size and morphology to sulfate-reducing bacteria, as has been observed in seep carbonates generated by anaerobic oxidation of methane (AOM) (e.g., van Lith et al., 2003; Barbieri and Cavalazzi, 2005; Peckmann et al., 2005; Reitner et al., 2005).

XRD analyses on bulk carbonate concretions from the study area showed that most of the studied carbonate samples were composed dominantly of pure calcite with small amounts of some impurities (goethite, quartz), agreeing well with our microscopic observations (Fig. 7; Table 1). Calcite content was as high as 95%, and quartz was the main detrital phase in these samples, at low

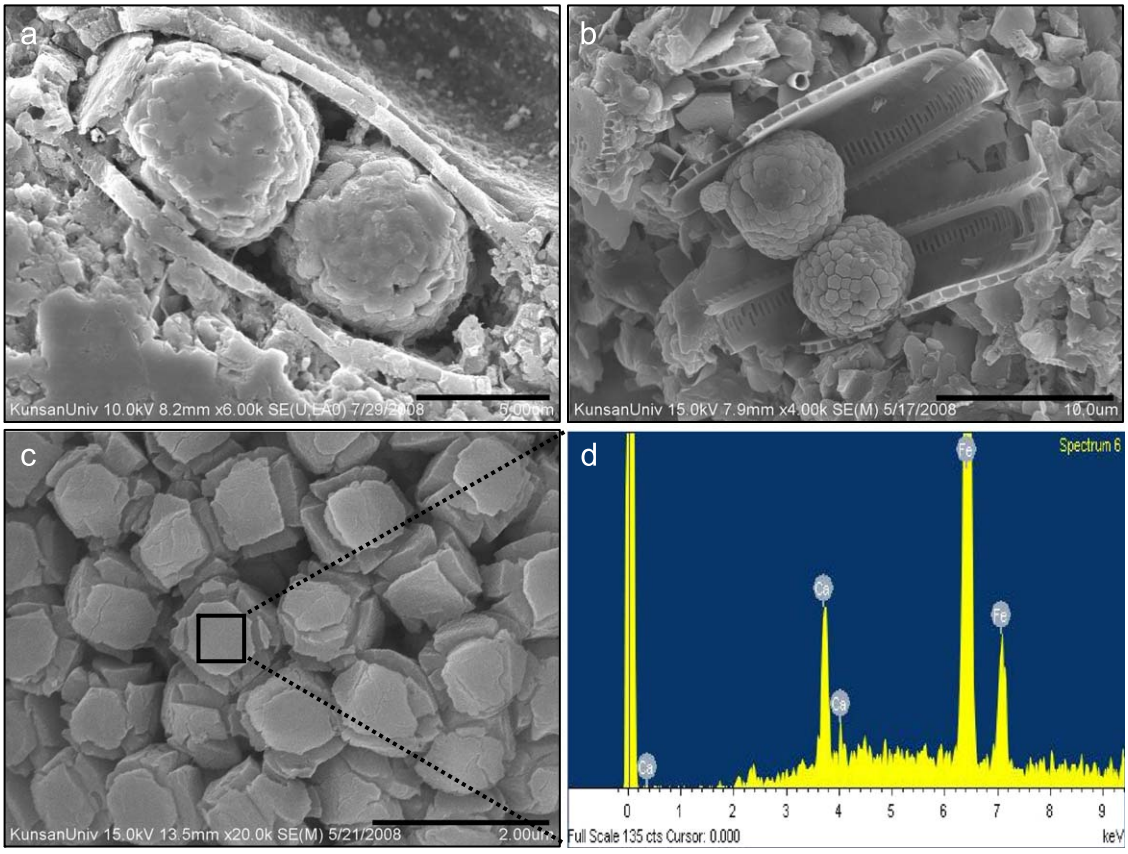

Fig. 5. SEM images showing (a) and (b) a representative agglomerate of euhedral siderite found in biological tests, and (c) well-crystallized siderite rhombs about 1 μm in size.

but stable amounts averaging about 5%. Notably, only one sample from the sediment layer of 31–32.5 cm was primarily composed of calcite (49%) and aragonite (47%) with minor quartz (3–4%; Table 1). In contrast, the carbonate concretions from the lowermost layer (237 cm) of the core were characterized by relatively low peak intensities of calcite and quartz compared to other studied samples, indicating relatively low crystallinity. On the other hand, the shift of $d(104)$ values away from that of stoichiometric calcite (3.035 Å) reflects the variable amounts of substitution of Mg^{2+} for Ca^{2+}. Most calcites in $d(104)$ value centered around 2.995 Å, indicating an $MgCO_3$ content of approximately 14 mol%. On the basis of this shift of the calcite peak (Lumsden and Chimahusky, 1980; Dickson, 2001), $MgCO_3$ contents in calcite were estimated to range from 10.7 to 14.3 mol% (Table 1), which correspond to high-Mg calcite (HMC, with $MgCO_3$ >5 mol%; Greinert et al., 2001).

Stable carbon and oxygen isotopes were measured in bulk authigenic carbonate samples, gas hydrate samples, and sediment void gas from core sediments (Table 2). Methane in gas hydrates, and sediment void gas were extremely depleted in ^{13}C, with $\delta^{13}C$ values ranging from −60.7‰ to −61.6‰ PDB. The $\delta^{13}C$ values for bulk authigenic carbonates ranged from −33.85‰ to −39.53‰ PDB, and $\delta^{18}O$ values mostly ranged between 5.16‰ and 5.60‰ PDB.

4. Discussion

4.1. Origin of carbonate concretions

The most characteristic feature of the carbonate samples analyzed in this study is the presence of abundant microbial structures within the carbonate matrix, together with their relatively high contents in HMC. Recent studies have shown that most methane derived from gas hydrate decomposition in marine sediments could seep upward the seafloor, then form seep communities dominated by tube worms and bivalves, which are dependent on endosymbiotic chemosynthetic bacteria (Aloisi et al., 2000; Peckmann et al., 2005; Chen et al., 2006). Therefore, identification of microbial structures and/or remnants of worm tubes within the carbonate matrix may represent useful indicators of methane seepage related to gas hydrate decomposition. Furthermore, the microcrystalline structure of carbonate minerals such as calcite, aragonite, and siderite has also been suggested as a reliable indicator of the authigenic origin of carbonate concretions from cold seep fluids (Druckman, 1981; Chfetz and Folk, 1984; Roberts et al., 1990; Lu et al., 2005; Chen et al., 2006). The mineralogy of the carbonate concretions from the gas-enriched sediments of the Ulleung Basin, East Sea, is dominated by HMC (Table 1). Average $MgCO_3$ contents (13.0 mol%) in the carbonate samples from the study area are comparable to those of methane-derived calcites from the eastern Mediterranean Sea (ca. 12 mol%; Aloisi et al., 2000), the northern Gulf of Mexico (6–21 mol%; Chen et al., 2007), Baffin Bay (14–18 mol%; Matsumoto, 1990), Monterey Bay (10–30 mol%; Stakes et al., 1999), and the Oregon/Washington subduction zone (average 12 mol%; Ritger et al., 1987). Accordingly, HMC in the study area may be typical methane-derived authigenic calcites, and the sources of Mg^{2+} could lie both in the methane-charged, rising fluids and/or in the bottom waters.

HMC precipitation may occur at various depths below the seafloor, in the sulfate reduction zone of marine sediments (Greinert et al., 2001; Bayon et al., 2007). In cold seep environments, however, it is commonly accepted that aragonite forms preferentially when the oxidation of methane-rich fluids occurs at

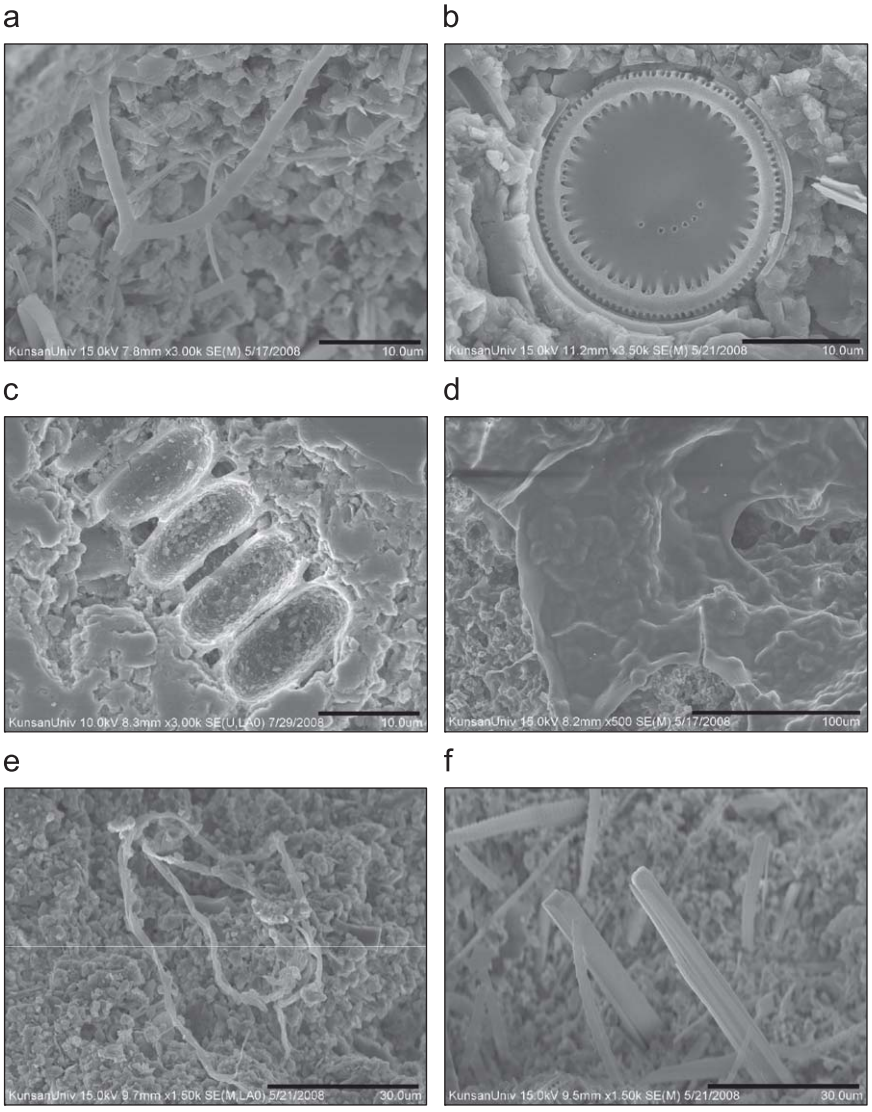

Fig. 6. Diversity of microbial structures preserved in authigenic carbonates, SEM microphotograhs. (a), (b) and (c) typical biological fossils, (d) biofilm (maybe algal mat), and (e) and (f) microbial activities (worm tube).

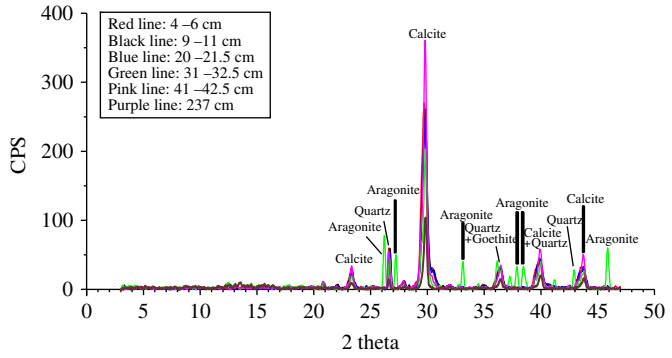

Fig. 7. X-ray diffraction patterns of bulk carbonate concretion samples. Note all the samples except for the sample of 31–32.5 cm show very similar pattern.

a close proximity to seawater, that is, in the near-seafloor environment (Burton and Walter, 1987; Ritger, et al., 1987; Burton, 1993; Bohrmann et al., 1998; Aloisi et al., 2000; Bayon et al., 2007). Previous studies have also shown that aragonite precipitation is favored over that of calcite at high SO_4^{2-} concentrations (Burton and Walter, 1987; Burton, 1993), and when uprising methane-rich fluids have a high velocity flow (Luff and Wallmann, 2003). Thus, the presence of aragonite at 31–32.5 cm depth suggests that carbonate precipitation in this layer took place near the seafloor. With the exception of carbonates from the sediment layer of 31–32.5 cm, the absence of aragonite in all other studied samples could be suggesting that aragonite actually never formed in the study area, or instead that it dissolved after initial precipitation (Burton, 1993; Luff et al., 2005; Bayon et al., 2007). Therefore, it is unclear whether the absence of aragonite-rich carbonate concretions in the Ulleung Basin sediments was caused by post-depositional dissolution and transformation processes or simply reflects that aragonite precipitation never took place.

4.2. Sources of diagenetic fluids and formation mechanism of authigenic carbonates

Carbon isotope composition of authigenic carbonates serves as an indicator for the origin of carbon incorporated during carbonate precipitation (Ritger et al., 1987; Takeuchi et al., 2002; Lu et al., 2005; Chen et al., 2006). Possible sources of carbon to the

Table 1
Mineral compositions of bulk carbonate concretions from core ROV07-4.

Core depth (cm)/sample number	Quartz (%)	Calcite (%)	Aragonite (%)	$MgCO_3$ in Calcite (mol%)
4–6	5	95	0	10.7
9–11	5	95	0	13.7
20–21.5	5	95	0	14.3
31–32.5/1	3	49	47	14.3
31–32.5/2	4	49	47	10.7
41–42.5	5	95	0	13.3
237/1	5	95	0	14.0
237/2	5	95	0	13.3

Table 2
Carbon and oxygen isotopic compositions of carbonate concretions, sediment void gas, and gas hydrate from core ROV07-4.

	Gas hydrate	Sediment void gas	Carbonate concretion						
Core depth (cm)/sample number	250–260	90	240	28/1	28/2	28/3	28/4	237/1	237/2
$\delta^{13}C$ (‰ PDB)	-61.2 ± 0.3 ($n=4$)	-61.6 ± 1.9 ($n=4$)	−60.7	−33.85	−33.87	−33.86	−33.86	−39.53	−39.53
$\delta^{18}O$ (‰ PDB)	–	–	–	5.28	5.16	5.32	5.33	5.31	5.60

pore fluids include: (1) biogenic methane ($\delta^{13}C<-65$‰ PDB) or thermogenic methane ($\delta^{13}C$ −30‰ to −50‰ PDB), (2) sedimentary organic carbon ($\delta^{13}C\sim-25$‰ PDB), and (3) marine biogenic carbonate or seawater CO_3^{2-} with a $\delta^{13}C$ value near 0‰ PDB (Anderson and Arthur, 1983; Aharon et al., 1997). Ultimately, the amount of mixing between these different components will determine the $\delta^{13}C$ value of any authigenic carbonate (Paull et al., 1992; Takeuchi et al., 2002). However, oxygen isotope ratios may provide information related to the temperature and origin of diagenetic fluids from which authigenic carbonates are precipitated. Authigenic carbonates from the study area showed low $\delta^{13}C$ (average −35.75‰ PDB) but high $\delta^{18}O$ values (average 5.33‰ PDB), obviously different from the $\delta^{13}C$ values of marine biogenic carbonate or seawater, indicating that the precipitates were predominantly methane-derived. Supporting this interpretation was the occurrence of other authigenic carbonate minerals (e.g., aragonite), which are usually correlated with microbially mediated anaerobic oxidation of methane (e.g., Lu et al., 2005). Therefore, these carbonate concretions likely formed near the sulfate–methane interface, at the location depth of the AOM.

Generally, methane in the marine environment can be generated through two main metabolic pathways: microbial methane ($\delta^{13}C$ <−65‰ PDB) formed by CO_2 reduction, and thermogenic methane ($\delta^{13}C$ −30‰ to −50‰ PDB) generated during organic matter maturation. In fact, the strongly depleted $\delta^{13}C$ values (ca. −61‰) of void gas extracted from the sediment samples, which was strikingly similar to the $\delta^{13}C$ value of the gas hydrate, indicates that the majority of the gas venting at the Ulleung Basin is microbial methane by CO_2 reduction ($CO_2+4H_2\rightarrow CH_4+2H_2O$). Fig. 8 shows that molecular compositions ($C_1/C_{2+}=2.4\sim3.2\times10^3$) and stable isotopic compositions ($\delta^{13}C_{CH4}=-60.7\sim-61.6$‰ PDB) of methane from sediment void and hydrate-bound gases fall in the field of microbial gas defined by Whiticar (1999). Gases originated either from the microbial CO_2 reduction or microbial fermentation of organic matter contain methane which is significantly depleted in ^{13}C ($\delta^{13}C_{CH4}$ <−55‰ PDB) and their molecular compositions (C_1/C_{2+}) are typically in the range of 10^3–10^5 (Whiticar, 1999; Milkov, 2005). Molecular ratios (C_1/C_{2+}) less than 50 and $\delta^{13}C_{CH4}$ of more than −50‰ PDB are typical for thermogenic methane (Clayton, 1991; Whiticar, 1999). However, authigenic carbonates from the study area yield carbon isotopic values that are approximately 20‰ PDB heavier than the methane of pore water, implying greater dilution of the dissolved inorganic carbon pool with carbon from other sources, e.g., microbial methane carbon diluted by dissolved inorganic carbon of seawater. Furthermore, the $\delta^{18}O$ values of the authigenic concretions in the study area ranged from 5.16‰ to 5.60‰ PDB, which are much higher than those (−29‰ to −30‰ PDB) of the bottom seawater around the study area, which is estimated from the regression line between salinity and $\delta^{18}O$ measured in surface water of the East Sea (Postlethwaite et al., 2005). It indicates that oxygen should come from the pore fluids enriched in ^{18}O (e.g., Aloisi et al., 2000; Takeuchi et al., 2002; Lu et al., 2005; Chen et al., 2007). Gas hydrate originating from microbial methane is mainly

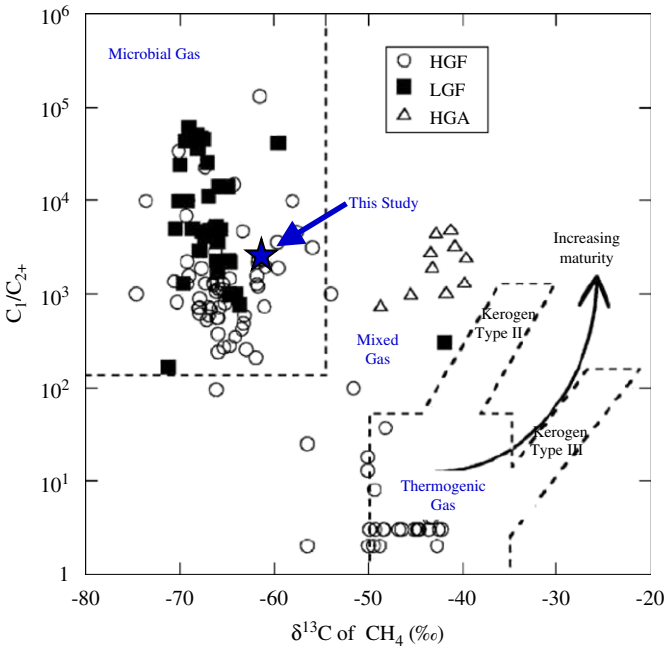

Fig. 8. Relationship between the ratio of C_1/C_{2+} hydrocarbons and stable carbon isotopic composition ($\delta^{13}C$) of methane in hydrate-bound gases from the global dataset subdivided into areas of high gas flux (HGF), low gas flux (LGF), and hydrate gas accumulations (HGF). Note that molecular and stable isotopic compositions of methane from current study fall in the field of microbial gas. The field of microbial, thermogenic and mixed gases are defined after Whiticar (1999) and basic frame of the figure and data are from Milkov (2005).

composed of methane with high $\delta^{18}O$ but very low $\delta^{13}C$ values, indicating that the authigenic concretions in the study area should be closely related to the fluids that originated from gas hydrate decomposition, especially for the carbonate samples collected in the lower section of the core (e.g., Bohrmann et al., 1998; Aloisi et al., 2000; Rodriguez et al., 2000; Greinert et al., 2001; Takeuchi et al., 2002; Chen et al., 2007). Accordingly, authigenic carbonate concretions from the study area are high-Mg calcite formed by AOM, which formed from the dissolution of gas hydrate. Because the marine bottom waters in the East Sea are usually oxic in nature, carbonate formation in these waters induced by the anaerobic oxidation of methane will be confined to anoxic sediments, especially in the Ulleung Basin, which has high organic carbon content (2.6–2.9%) and sulfate reduction rate (0.72–1.89 mmol m^{-2} day^{-1}; Lee et al., 2008). As a result, the active cold (i.e., methane) seepage area of the Ulleung Basin in the East Sea is characterized by AOM in the shallow subsurface, leading to the oversaturation of pore fluids with respect to carbonate, and consequently to the precipitation of authigenic carbonate minerals.

5. Conclusions

Abundant carbonate concretions were found in gas-hydrate-bearing sediments from the western slope area of the Ulleung Basin (East Sea). These carbonates are dominated by authigenic, micritic HMC with small amounts of some impurities (goethite and quartz). Isotopic compositions of the carbonate samples are characterized by strongly depleted ^{13}C and obviously enriched ^{18}O, with $\delta^{13}C$ values from −33.85‰ to −39.53‰ PDB and $\delta^{18}O$ values range from 5.16‰ to 5.60‰ PDB. The carbon isotopic compositions, together with SEM observation and mineralogical composition, demonstrate that these carbonates precipitated from dissolved inorganic carbon produced by microbially mediated anaerobic oxidation of methane. Moreover, the very high oxygen isotopic compositions of the diagenetic carbonates indicate that precipitation occurred with bottom seawaters mixed with a variable contribution of water from gas hydrate decomposition. Consequently, this study showed that the deep-sea floor of the Ulleung Basin, East Sea, is a site of cold seeps, methane degassing and bacterially mediated precipitation of HMC.

Acknowledgements

This study was supported by grants to KORDI research programs (Grant no PM50101, PE9830u) in Korea. The authors are grateful to Mrs. K.C. Rho and T. H. Lee of the Korea Ocean Research and Development Institute (KORDI), who kindly assisted with the laboratory works. Critical comments by two anonymous reviewers on the original manuscript are highly appreciated.

References

Aharon, P., Schwarcz, H.P., Roberts, H.H., 1997. Radiometric dating of submarine hydrocarbon seeps in the Gulf of Mexico. GSA Bulletin 109, 568–579.

Aloisi, G., Pierre, C., Rouchy, J.M., Foucher, J.P., Woodside, J., 2000. Methane-related authigenic carbonates of eastern Mediterranean Sea mud volcanoes and their possible relation to gas hydrate destabilisation. Earth and Planetary Science Letters 184, 321–338.

Anderson, T.F., Arthur, M.A., 1983. Stable isotopes of oxygen and carbon and their application to sedimentologic and paleoenvironmental problems. In: Arthur, M.A., Anderson, R.F., Kaplan, I.R., Veizer, J. (Eds.), Stable Isotopes in Sedimentary Geology, 10. SEPM Short Course, pp. 111–151.

Bayon, G., Pierre, C., Etoubleau, J., Voisset, M., Cauquil, E., Marsset, T., Sultan, N., Le Drezen, E., Fouquet, Y., 2007. Sr/Ca and Mg/Ca ratios in Niger Delta sediments: implications for authigenic carbonate genesis in cold seep environments. Marine Geology 241, 93–109.

Barbieri, R., Cavalazzi, B., 2005. Microbial fabrics from Neogene cold seep carbonates, Northern Apennine, Italy. Palaeogeography Palaeoclimatology Palaeoecology 227, 143–155.

Boetius, A., Ravenschlag, K., Schubert, C.J., Rickert, D., Widdel, F., Gieseke, A., Amann, R., Jorgensen, B.B., Whitte, U., Pfannkuche, O., 2000. A marine consortium apparently mediating anaerobic oxidation of methane. Nature 407, 623–626.

Bohrmann, G., Meinert, J., Suess, E., Torres, M., 1998. Authigenic carbonates from the Cascadia subduction zone and their relation to gas hydrate stability. Geology 26, 647–650.

Burton, E.A., 1993. Controls on marine carbonate cement mineralogy: review and reassessment. Chemical Geology 105, 163–179.

Burton, E.A., Walter, L.M., 1987. Relative precipitation rates of aragonite and Mg calcite from sea water: temperature or carbonate ion control? Geology 15, 111–114.

Chen, Y.F., Matsumoto, R., Paull, C.K., Ussler III, W., Lorenson, T., Hart, P., Winters, W., 2007. Methane-derived authigenic carbonates from the northern Gulf of Mexico—MD02 Cruise. Journal of Geochemical Exploration 95, 1–15.

Chen, Z., Yan, W., Chen, M.H., Wang, S.H., Lu, J., Zhang, F., Xiang, R., Xiao, S.B., Yan, P., Gu, S.C., 2006. Discovery of seep carbonate nodules as new evidence for gas venting on the northern continental slope of South China Sea. Chinese Science Bulletin 51, 1228–1237.

Chfetz, H.S., Folk, R.L., 1984. Travertines: Depositional morphology and the bacterially constructed constituents. Journal of Sedimentary Petrology 54, 289–316.

Clayton, C., 1991. Carbon isotope fractionation during natural gas generation from kerogen. Marine and Petroleum Geology 8, 232–240.

Dickson, J.A.D., 2001. Transformation of echinoid Mg calcite skeletons by heating. Geochimica et Cosmochimica Acta 3, 443–454.

Druckman, Y., 1981. Subrecent manganese-bearing stromatolites along shorelines of the Dead Sea in Phanerozoic Stromatolites. In: Monty, C. (Ed.), Phanerozoic Stromatolites. Springer, Berlin, pp. 197–208.

Ferdelman, T.G., Lee, C., Pantoja, S., Harder, J., Bebout, B.M., Fossing, H., 1997. Sulfate reduction and methanogenesis in a Thioploca-dominated sediment off the coast of Chile. Geochimica et Cosmochimica Acta 61, 3065–3079.

Gardner, J.M., Shor, A.N., Jung, W.Y., 1998. Acoustic imagery evidence for methane hydrates in the Ulleung Basin. Marine Geophysical Research 20, 495–503.

Greinert, J., Bohrmann, G., Suess, E., 2001. Gas hydrate-associated carbonates and methane-venting at Hydrate Ridge: Classification, distribution, and origin of authigenic lithologies. In: Paull, C.K., Dillon, W.P. (Eds.), Natural Gas Hydrates: Occurrence, Distribution, and Detection. American Geophysical Union, Washington, DC, pp. 99–114.

Greinert, J., Bollwerk, S.M., Derkachev, A., Bohrmann, G., Suess, E., 2002. Massive barite deposits and carbonate mineralization in the Derugin Basin, Sea of Okhotsk: precipitation processes at cold seep sites. Earth and Planetary Science Letters 203, 165–180.

Han, Z., Suess, E., Huang, Y., Wu, N., Bohrmann, G., Su, S., Eisenhauer, A., Rehder, G., Fang, Y., 2008. Jiulong methane reff: microbial mediation of seep carbonates in the South China Sea. Marine Geology 249, 243–256.

Horozal, S., Lee, G., Yi, B., Yoo, D., Park, K., Lee, H., Kim, W., Kim, H., Lee, K., 2009. Seismic indicators of gas hydrate and associated gas in the Ulleung Basin, East Sea (Japan Sea) and implication of heat flows derived from depths of the bottom-simulating reflector. Marine Geology 258, 126–138.

Lee, T., Hyun, J., Mok, J.S., 2008. Organic carbon accumulation and sulfate reduction rates in slope and basin sediments of the Ulleung Basin, East/Japan Sea. Geo-Marine Letters 28, 153–159.

Lu, H.F., Liu, J., Chen, F., Liao, Z.L., Sun, X.M., Su, X., 2005. Mineralogy and stable isotopic composition of authigenic carbonates in bottom sediments in the offshore area of southwest Taiwan, South China Sea: evidence for gas hydrate occurrence. Earth Science Frontiers (in Chinese with English abstract) 12, 268–276.

Luff, R., Greinert, J., Wallmann, K., Klaucke, I., Suess, E., 2005. Simulation of long-term feedbacks from authigenic carbonate crust formation at cold vent sites. Chemical Geology 216, 157–174.

Luff, R., Wallmann, K., 2003. Fluid flow, methane fluxes, carbonate precipitation and biogeochemical turnover in gas hydrate-bearing sediments at Hydrate Ridge, Cascadia Margin: numerical modeling and mass balances. Geochimica et Cosmochimica Acta 67, 3403–3421.

Lumsden, D.N., Chimahusky, J.S., 1980. Relationship between dolomite nonstoichiometry and carbonate facies parameters. In: Zenger, D.H., Dunham, J.B., Ethington, R.L. (Eds.), Concepts and Models of Dolomitizaion, 28. SEPM Special Publication, pp. 123–137.

Matsumoto, R., 1990. Vuggy carbonate crust formed by hydrocarbon seepage on the continental shelf of Vaffin Island, northeast Canada. Geochemical Journal 24, 143–158.

Mazzini, A., Ivanov, M., Parnell, J., Stadnitskaia, A., Cronin, B.T., Poludetkina, E., Mazurenko, L., van Weering, T.C.E., 2004. Methane-related authigenic carbonates from the Black Sea: geochemical characterization and relation to seeping fluids. Marine Geology 212, 153–181.

McCrea, C.M., 1950. The isotopic chemistry of carbonates and a paleotemperature scale. Journal of Chemical Physics 18, 849–857.

Milkov, A.V., 2005. Molecular and stable isotope compositions of natural gas hydrates: a revised global dataset and basic interpretations in the context of geological settings. Organic Geochemistry 36, 681–702.

Ohta, K., Terai, H., Kimura, I., Tanaka, K., 1999. Simultaneous determination of hydrogen, methane, and carbon monoxide in water by gas chromatography with a semiconductor detector. Analytical Chemistry 71, 2697–2699.

Paull, C.K., Chanton, J.P., Neumann, A.C., Coston, J.A., Martens, C.S., 1992. Indicators of methane-derived carbonates and chemosynthetic organic carbon deposits: examples from the Florida escarpment. Palaios 7, 361–375.

Peckmann, J., Little, C.T.S., Gill, F., 2005. Worm tube fossils from the Hollard Mound hydrocarbon-seep deposit, Middle Devonian, Morocco: Palaeozoic seep-related vestimentiferans? Palaeogeography Palaeoclimatology Palaeoecology 227, 242–257.

Peckmann, J., Reimer, A., Luth, U., Luth, C., Hansen, B.T., Heinicke, C., Hoefs, J., Reitner, J., 2001. Methane-derived carbonates and authigenic pyrite from the northwestern Black Sea. Marine Geology 177, 129–150.

Postlethwaite, C.F., Rohling, E.J., Jenkins, W.J., Walker, C.F., 2005. A tracer study of ventilation in the Japan/East Sea. Deep-Sea Research II 52, 1684–1704.

Reitner, J., Peckmann, J., Blumenberg, M., Michaelis, W., Reimer, A., Thiel, V., 2005. Concretionary methane-seep carbonates and associated microbial communities in Black Sea sediments. Palaeogeography Palaeoclimatology Palaeoecology 223, 18–30.

Ritger, S., Carson, B., Suess, E., 1987. Methane-derived authigenic carbonates formed by subduction-induced pore-water expulsion along the Oregon/Washington margin. Geological Society of America Bulletin 98, 147–156.

Roberts, H.H., Aharon, P., Carney, R., Larkin, J., Sassen, R., 1990. Seafloor responses to hydrocarbon seeps, Louisiana continental slope. Geo-Marine Letters 10, 232–243.

Rodriguez, N.M., Paull, C.K., Borowski, W.S., 2000. Zonation of authigenic carbonates within gas hydrate-bearing sedimentary sections on the Blake Ridge: Offshore southeastern North America. In: Paull, C.K., Matsumoto, R., Wallace, P.J., Dillon, W.P. (Eds.), Proceedings of the Ocean Drilling Program, Scientific Results, 164 (Ocean Drilling Program). College Station, TX, pp. 301–313.

Sharma, T., Clayton, R.N., 1965. Measurement of 18O/16O ratios of total oxygen in carbonates. Geochimica et Cosmochimica Acta 29, 1347–1353.

Stakes, D.S., Orange, D., Paduan, J.B., Salamy, K.A., Maher, N., 1999. Cold seep and authigenic carbonate formation in Monterey Bay, California. Marine Geology 159, 93–109.

Stein, R., Schubert, C., Vogt, C., Fterer, D., 1994. Stable isotope stratigraphy, sedimentation rates, and salinity changes in the latest Pleistocene to Holocene eastern central Arctic Ocean. Marine Geology 119, 335–355.

Takeuchi, R., Machiyama, H., Matsumoto, R., 2002. Methane seep, chemosynthetic communities, and carbonate crusts on the Kuroshima Knoll, offshore Ryukyu islands. In: Proceedings of the Fourth International Conference on Gas Hydrate. Yokohama, pp. 97–101 (May 19–23).

Tsunogai, U., Yoshida, N., Gamo, T., 2002. Carbon isotopic evidence of methane oxidation through sulfate reduction in sediment beneath cold seep vents on the seafloor at Nankai Trough. Marine Geology 187, 145–160.

van Lith, Y., Warthmann, R., Vasconcelos, C., Mckenzie, J.A., 2003. Microbial fossilization in carbonate sediments: a result of the bacterial surface involvement in dolomite formation. Sedimentology 50, 237–245.

Whiticar, M.J., 1999. Carbon and hydrogen isotope systematics of bacterial formation and oxidation of methane. Chemical Geology 161, 291–314.

Geo-Mar Lett
DOI 10.1007/s00367-009-0142-x

ORIGINAL

Rare earth elements in bottom sediments of major rivers around the Yellow Sea: implications for sediment provenance

Zhaokai Xu · Dhongil Lim · Jinyong Choi · Shouye Yang · Hoisoo Jung

Received: 12 January 2009 / Accepted: 29 April 2009

Abstract Rare earth elements (REEs) of 91 fine-grained bottom sediment samples from five major rivers in Korea (the Han, Keum, and Yeongsan) and China (the Changjiang and Huanghe) were studied to investigate their potential as source indicator for Yellow Sea shelf sediments, this being the first synthetic report on REE trends for bottom sediments of these rivers. The results show distinct differences in REE contents and their upper continental crust (UCC)-normalized patterns: compared to heavy rare earth elements (HREEs), light rare earth elements (LREEs) are highly enriched in Korean river sediments, in contrast to Chinese river sediments that have a characteristic positive Eu anomaly. This phenomenon is observed also in primary source rocks within the river catchments. This suggests that source rock composition is the primary control on the REE signatures of these river sediments, due largely to variations in the levels of chlorite and monazite, which are more abundant in Korean bottom river sediments. Systematic variations in ΣLREE/ΣHREE ratios, and in (La/Yb)–$(Gd/Yb)_{UCC}$ but also (La/Lu)–$(La/Y)_{UCC}$ and (La/Y)–$(Gd/Lu)_{UCC}$ relations have the greatest discriminatory power. These findings are consistent with, but considerably expand on the limited datasets available to date for suspended sediments. Evidently, the REE fingerprints of these river sediments can serve as a useful diagnostic tool for tracing the provenance of sediments in the Yellow Sea, and for reconstructing their dispersal patterns and the circulation system of the modern shelf, as well as the paleoenvironmental record of this and adjoining marginal seas.

Z. Xu · J. Choi
Department of Oceanography, Kunsan National University, Kunsan 573-701, Korea

Z. Xu
Key Laboratory of Marine Geology and Environment, Institute of Oceanology, Chinese Academy of Sciences, Qingdao 266071, China

D. Lim (✉)
South Sea Research Institute,
Korea Ocean Research and Development Institute,
391 Jangmok-ri Jangmok-myun,
Geoje 656-830, Korea
e-mail: oceanlim@kordi.re.kr

S. Yang
Laboratory of Marine Geology, Tongji University, Shanghai 200092, China

H. Jung
Marine Geoenvironment and Resources Research Division,
Korea Ocean Research and Development Institute,
Ansan, P.O. Box 29, Seoul 425-600, Korea

Published online: 16 May 2009

Introduction

The Yellow Sea, located at the northern tip of the western Pacific and surrounded by Korea and China, is a typical epicontinental marginal sea (Fig. 1) that annually receives approx. 10% of the world's riverine sediment discharge (Milliman and Meade 1983). This massive sedimentary load comes principally from two of the world's largest rivers, the Changjiang and the Huanghe of China, with smaller contributions from Korean rivers such as the Han, the Keum, and the Yeongsan. Geological research on Yellow Sea sediments has encompassed both the modern and paleo-sedimentary domains (e.g., Chough and Kim 1981; Nittrouer et al. 1984; Milliman et al. 1985; Alexander et al. 1991; Liu et al. 2006, 2007; Lim et al. 2007; Yang and Liu 2007), with some studies focusing more on geochemical proxies of sediment source (e.g., Cho et al. 1999; Kim et al. 1999; Yang et al. 2002a; Lim et al. 2006; Yang and

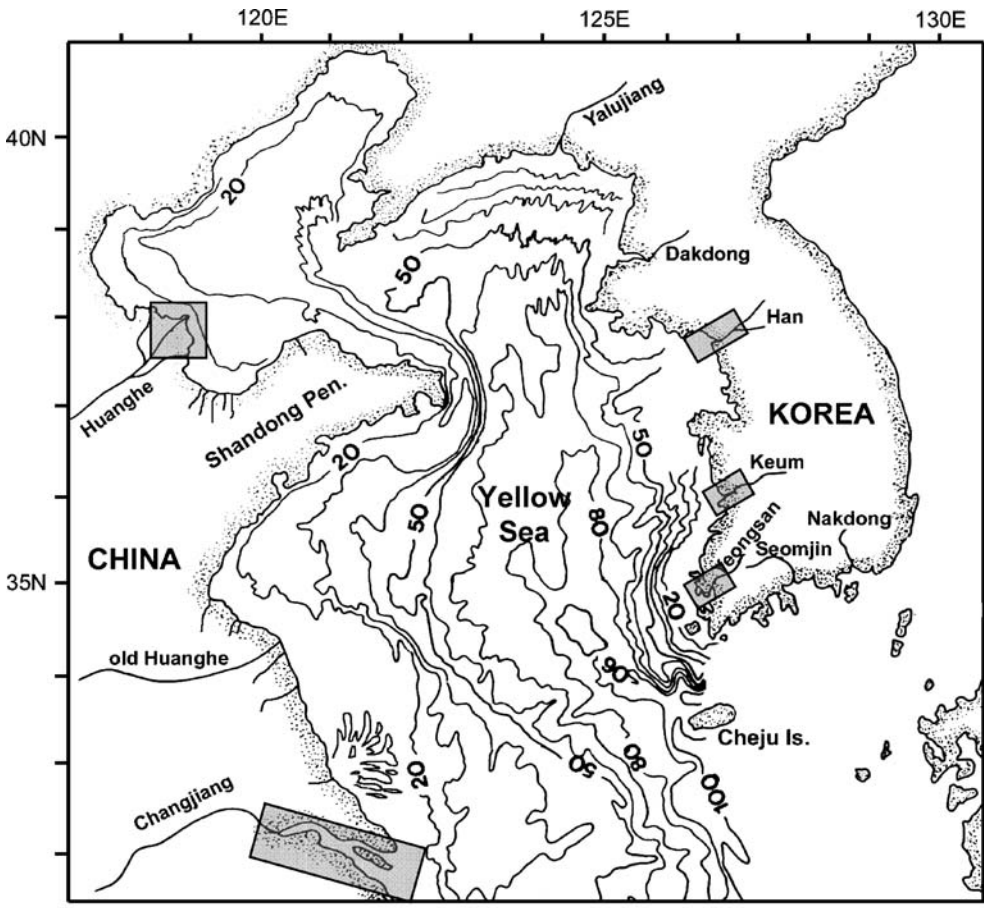

Fig. 1 Locality map showing the major Korean (Han, Keum, and Yeongsan) and Chinese rivers (Changjiang and Huanghe) entering the Yellow Sea, and the sampling areas (*shaded*). Isobaths are in meters

Youn 2007). This wealth of information has provided an excellent model of an epicontinental shelf setting that is helpful for interpreting the world's stratigraphic record. Nevertheless, the multifaceted origin of Yellow Sea sediments, as well as associated dispersal pathways, sediment budgets, and sedimentation rates are still controversial, as noted already by Yang et al. (2003a) in their comprehensive review, notably for the Huanghe River (Su and Huh 2002). Although it has long been generally considered that Chinese rivers (Changjiang, Huanghe) are the major sources of sediments accumulating on the Yellow Sea shelf, supply by Korean rivers has very recently been shown to be more important and associated with wider dispersal than commonly thought to date (Liu et al. 2009). In addition, the occurrence of Chinese riverine sediments in the central south, and even the eastern part of the Yellow Sea has been argued by some researchers (e.g., Park et al. 2000; Lee and Chu 2001; Yang et al. 2003a; Lan et al. 2007; Lim et al. 2007; Wang et al. 2007).

Yang et al. (2003a) and, more recently, Lim et al. (2006) have shown that previously used mineralogical and geochemical indices such as smectite, vanadium, and $CaCO_3$ contents, and some major elemental ratios have not proved effective in identifying sediment provenance in the Yellow Sea, because of limited attention paid to grain-size effects and dilution by biogenic materials, and insufficient accompanying data on potential source end-members. Given the remarkable differences in drainage basin rock compositions and weathering patterns among Korean and Chinese rivers, noted by, e.g., Yang et al. (2003b, 2007) and Lim et al. (2006), one alternative is the use of rare earth elements (REEs) as diagnostic proxy. Generally, REEs are characterized by strong partitioning into the particulate phase; coherent behavior during weathering, erosion, and fluvial transportation; and high resistance to chemical mobilization. Thus, their contents in marine sediments are controlled largely by the competing influences of provenance, mineralogical character, and to a lesser extent, chemical weathering intensity (McLennan 1989), with only limited effects from sediment grain size and biogenic material enrichment (Zhu et al. 1997; Yang et al. 2002b, 2003b; Lee et al. 2008). Because of this, REEs have been widely used as potentially excellent tracers for determining sediment source in numerous settings, including the Bohai, Yellow, and East

China seas (e.g., Goldstein and Jacobsen 1988; Elderfield et al. 1990; Klaver and van Weering 1993; Yang et al. 2002b; Munksgaard et al. 2003; Lin et al. 2008).

In the Yellow Sea, Nohara et al. (1999) suggested that variable sediment sources could not be easily distinguished based on their findings of uniform REE patterns and similar fractionations for some scattered bottom sediment samples. Other studies have successfully used REEs to discriminate between river sediment input via the Changjiang and Huanghe rivers of China (Zhang et al. 1998, the Changjiang River; Yang et al. 2002b, and Jiang et al. 2009, the Changjiang and Huanghe rivers). Based on REE data of suspended matter collected in both Korean and Chinese rivers, Yang et al. (2003b) reported that, compared to the loads of the Changjiang, Huanghe and Yalujiang rivers of China, those of the Han, Keum and Yeongsan rivers of Korea showed enrichment of light rare earth elements (LREEs) relative to the upper continental crust (UCC), and distinct (La/Yb)–$(Gd/Yb)_{UCC}$ signatures. Yet, these findings are based on only 15 samples, too few for these trends to be automatically accepted as representative for these five rivers. Likewise, the distinct REE patterns reported by Liu et al. (2009) for the Changjiang and Huanghe rivers, and for rivers on the Korean Peninsula stem from only one core recovered off the Shandong Peninsula of China.

Evidently, large-scale but nevertheless sufficiently detailed geochemical investigations incorporating the REE signatures of riverine bottom sediments for all main potential source end-members in the Yellow Sea are still lacking. Particularly in view of the pronounced man-induced decrease in sediment load and runoff caused by the construction of the Three Gorges Dam across the Changjiang River (see below), such broader-scale high-resolution baseline studies are today urgently needed.

Within this context, this study investigated the REE compositions of bottom sediments from five major Korean and Chinese rivers and/or estuaries that connect directly to the Yellow Sea, with the aim of establishing typical regional-scale REE fingerprints that could prove useful in sediment source discrimination in this and adjoining marginal seas.

Physical setting

The drainage basins of the three Korean rivers (the Han, Keum, and Yeongsan, $<4\times10^4$ km^2 combined) are considerably smaller than those of the Chinese rivers (the Huanghe and Changjiang, $>2\times10^6$ km^2 combined) investigated in this study. The Han River system, the largest in South Korea in terms of both water discharge and total river length, drains approx. 2.6×10^4 km^2, and has a sediment discharge of 2 to 12.4×10^6 tons/year. The Keum and Yeongsan rivers drain approx. 9.9×10^3 and 2.8×10^3 km^2, respectively, with discharges varying from 1 to 11×10^6 tons/year (Lim et al. 2007). The Korean river basins are dominated by Jurassic and Cretaceous granites, Precambrian gneiss, and loose Quaternary sediments, with only rare carbonates (Park et al. 2007; Lee et al. 2008).

The Chinese river drainage basins differ substantially in geologic and geographic settings, and in prevailing climate (Zhang et al. 1990a; Chen et al. 2000). The Changjiang, draining about 1.8×10^6 km^2 and with approx. 0.5×10^9 tons/year sediment discharge up to the 1980 s (Chen et al. 2008), flows in central and east China along the edge of the high-precipitation monsoon region. Its basin has a basement rock complex consisting of Paleozoic carbonate rocks in the upper reaches, and acidic-metamorphic rocks and Quaternary clastic sediments in the middle and lower reaches. Most Changjiang sediments come from the weathered materials (i.e., carbonate rock) of the upper reaches, especially those around Jinshajiang (Wang et al. 1994; Yang et al. 2002b). By contrast, the Huanghe, draining about 0.8×10^6 km^2 and with sediment discharge sometimes reaching 1×10^9 tons/years, flows across the dry Loess Plateau of north China. Approximately 90% of Huanghe sediments originate from this plateau, situated along the middle reaches of the river, and occupying about half of its drainage basin (Ren and Shi 1986; Zhang et al. 1990b).

Since the late Quaternary, the routes, runoffs, and sediment loads of these rivers, particularly the Chinese rivers, have seen considerable changes, some man-induced. These include the shift of the Huanghe drainage system from the southern Yellow Sea into the northern Yellow Sea (the Bohai Sea) about 150 years ago (Ren and Shi 1986). Of special concern more recently is the construction of the Three Gorges Dam in the upper reaches of the Changjiang River, and its dramatic impact on river discharge and associated pressure on the coastal zone (e.g., Xu and Milliman 2009). According to Chen et al. (2008), sediment loads from the Changjiang averaged about 3.5×10^8 tons/year before the construction of the dam commenced in late 1994, but this has possibly decreased to about 1.1×10^6 tons/year since the closure of the dam in 2008. This means that, in terms of sediment budgets for the Yellow and East China Sea shelf, the relative contribution of Korean rivers will substantially increase in future.

Materials and methods

In all, 91 surface sediment samples were collected from major riverine sediment source areas on mainland Korea and China, as well as their nearby coastal areas (Fig. 1): 31 samples from the Han, Keum, and Yeongsan rivers of

Korea in 2005, and 60 samples from the Changjiang and Huanghe of China in the late 1990 s and 2006, respectively. Sediments in the 490-km-long Han River were collected in its lower reaches, from the mouth to about 50 km upstream, as well as at 250–300 km from the mouth. Sampling sites along the 400-km-long Keum and 120-km-long Yeongsan rivers extended from the river mouths to 30–50 km upstream. Sites along the 6,300-km-long Changjiang and 5,400-km-long Huanghe ranged from the river mouths to 200–300 km upstream, corresponding to the lower reaches of these rivers. Coastal or deltaic sediments were also sampled 10–50 km offshore from the Chinese rivers, all in less than 30 m of water. Except for two samples from the upper basin of the Han River, this study focuses on fine-grained bottom sediments from the lower reaches of the five main rivers debouching into the central/southern Yellow Sea.

For REE (La, Ce, Pr, Nd, Sm, Eu, Gd, Dy, Ho, Er, Yb, Lu, and Y) analyses, the bulk sediments were oven-dried at 60°C overnight, and then powdered and homogenized with an automated agate mortar and pestle. In each case, about 0.2 g of powdered sample was weighed into a graphite crucible, and admixed with 1.0 g $LiBO_2$. These mixtures were then fused at 900°C for 20 min, and the resultant cake was cooled and dissolved in 200 ml cold 5% nitric acid (HNO_3). Each solution was analyzed for REE contents using inductively coupled plasma mass spectrometry (ICP-MS; Perkin-Elmer ELAN 5000) at the University of London. The detection limits ranged from 0.1 to 0.5 μg/g for La, Sm, Eu, Gd, Dy, Ho, Er, Yb, and Lu, and to 1 μg/g for Ce, Pr, Nd, and Y.

The validity of the analytical procedure was evaluated by accuracy and precision tests conducted on the reference sample MAG-1 provided by the United States Geological Survey. The results show that relative deviations between measured and certified values were generally less than 10% (Table 1), indicating satisfactory recoveries.

Normalization to the upper continental crust is a widely accepted method of comparing the REE contents of various geological materials (cf. Taylor and McLennan 1985), and this approach was used throughout this study.

Table 1 Analyses of standard reference material (MAG-1) for REE contents

Element (μg/g)	Recommended value[a]	Measured value (n=23)	2σ	α
La	43	39.6	1.38	8
Ce	88	81.6	3.45	7
Pr	–	9.1	0.33	–
Nd	38	38.3	1.56	1
Sm	7.5	7.1	0.33	5
Eu	1.6	1.5	0.11	9
Gd	5.8	5.4	0.43	7
Dy	5.2	4.6	0.22	12
Ho	1	0.9	0.05	13
Er	–	2.3	0.15	–
Yb	2.6	2.3	0.12	10
Lu	0.4	0.4	0.02	11
Y	28	27.2	1.28	3

[a] Standard value of reference material (MAG-1) recommended by the United States Geological Survey for the validity of the analytical procedure; 2σ is the standard deviation of measured values; α is the accuracy, estimated as $[1 - (\text{element}_{\text{measured in reference}} / \text{element}_{\text{recommended for standard}}) \times 100]$

Results

In all river sediments, Ce, La, Nd, and Y are the predominant elements (Table 2). Moreover, LREEs (La to Eu) are more enriched than heavy rare earth elements (HREEs; Gd to Lu, and Y). The REE contents of most river sediments are fairly uniform, with coefficients of variation (CVs) lower than 10% (Fig. 2). However, the Huanghe sediments have CVs higher than 15%, reflecting large variations in REE contents. Mean total REE contents (∑REE) are highest in the Han and Keum river sediments of Korea, and lowest in the Huanghe sediments of China (Table 2). Furthermore, mean total LREE contents (∑LREE) are much lower in the Chinese river samples. By contrast, mean total HREE contents (∑HREE) are similar in the rivers of both countries (Table 3).

REE fractionation is more pronounced in the Korean than in the Chinese river sediments, especially the Huanghe. ∑LREE/∑HREE ratios range from 3.15 to 3.80 (mean 3.44±0.16) for the Chinese river sediments, but from 4.26 to 4.81 (mean 4.50±0.16) for the Korean river sediments (Table 3).

In terms of UCC-normalized distributions, the Korean sediments exhibit a rather distinct LREE plateau from La to Eu (Fig. 3). In particular, these sediments are characterized by strong LREE enrichment with obvious REE fractionation. By contrast, the Chinese river sediments show a convex trend in terms of atomic number, with enrichment in the middle-REEs (Nd, Sm, and Eu), and depletion of the other LREEs and HREEs. This convex fractionation pattern is more pronounced in the Changjiang sediments, especially for Eu; the Huanghe sediments show a reduced convexity due to their Sm-positive values, without obvious REE fractionation.

Normalized values of $(La/Yb)_{UCC}$ in the Korean river sediments range from 1.25 to 1.56, with a mean of 1.39±0.09; in the Chinese river sediments, the range is 0.81 to 1.22, with a mean of 0.99±0.08 (Table 3). All other

Table 2 Summary of REE contents (μg/g) in bottom sediments of five rivers in Korea and China, together with some important fractionation ratios

	Korean rivers												Chinese rivers							
	Han River (n=6)				Keum River (n=13)				Yeongsan River (n=12)				Changjiang (n=18)				Huanghe (n=42)			
	Min.[a]	Max.	Mean	SD	Min.	Max.	Mean	SD	Min.	Max.	Mean	SD	Min.	Max.	Mean	SD	Min.	Max.	Mean	SD
La	43.02	56.95	48.81	5.27	40.76	57.35	49.07	3.84	40.66	46.42	43.79	1.83	33.09	41.81	37.87	2.46	23.10	45.79	31.33	4.78
Ce	86.00	113.34	96.76	10.43	80.00	112.91	96.65	8.00	82.01	94.19	88.50	4.34	67.98	87.28	77.65	5.58	45.98	92.63	63.88	10.26
Pr	9.15	11.49	10.16	0.91	8.71	12.22	10.23	0.89	8.74	10.26	9.40	0.44	7.22	9.39	8.39	0.61	5.12	10.07	6.94	1.11
Nd	37.20	46.24	41.68	3.41	36.96	49.23	42.65	3.44	36.22	41.67	38.57	1.61	30.17	41.16	35.49	2.67	22.12	42.49	29.29	4.54
Sm	6.40	7.95	7.07	0.63	5.73	8.12	7.18	0.60	6.17	7.29	6.85	0.35	5.44	7.13	6.47	0.43	3.95	7.85	5.48	0.85
Eu	1.10	1.49	1.26	0.13	1.20	1.62	1.43	0.14	1.27	1.50	1.41	0.07	1.11	1.69	1.39	0.17	0.79	1.28	1.05	0.12
Gd	4.77	5.68	5.22	0.39	4.13	5.76	5.13	0.46	4.29	5.45	4.80	0.32	4.16	5.57	4.85	0.36	2.96	6.10	4.23	0.66
Dy	4.05	5.12	4.62	0.43	3.91	5.15	4.59	0.35	4.18	4.76	4.39	0.18	4.10	5.21	4.65	0.29	3.00	5.77	4.07	0.62
Ho	0.74	0.92	0.85	0.07	0.70	1.01	0.88	0.08	0.81	0.91	0.85	0.03	0.82	1.07	0.92	0.08	0.57	1.12	0.80	0.11
Er	2.11	2.55	2.37	0.18	2.11	2.74	2.40	0.18	2.13	2.56	2.30	0.12	2.19	2.77	2.50	0.17	1.60	3.15	2.20	0.33
Yb	2.32	2.71	2.52	0.17	2.24	2.83	2.51	0.20	2.26	2.65	2.44	0.14	2.38	2.90	2.61	0.15	1.79	3.69	2.43	0.41
Lu	0.33	0.39	0.37	0.02	0.32	0.49	0.39	0.04	0.33	0.44	0.36	0.03	0.36	0.48	0.40	0.03	0.23	0.59	0.37	0.07
Y	27.07	32.32	29.77	2.30	24.92	33.02	29.37	2.62	25.73	30.12	27.58	1.33	27.18	33.77	30.63	1.90	18.66	39.05	26.74	4.26
∑REE	226.51	286.86	251.46	23.81	212.10	291.18	252.50	20.04	216.05	246.96	231.24	9.78	186.38	237.25	213.83	14.26	130.34	256.56	178.80	27.71
∑LREE	184.12	237.46	205.74	20.63	173.37	240.86	207.23	16.55	175.78	200.83	188.52	8.25	145.00	187.82	167.27	11.65	101.28	200.00	137.97	21.53
∑HREE	41.64	49.40	45.72	3.47	38.73	50.32	45.28	3.72	40.27	46.13	42.72	1.90	41.38	50.75	46.56	2.78	29.06	59.42	40.83	6.34
∑LREE/∑HREE	4.26	4.81	4.50	0.19	4.36	4.79	4.58	0.14	4.27	4.74	4.41	0.14	3.43	3.80	3.59	0.10	3.15	3.78	3.38	0.13
$(La/Yb)_{UCC}$	1.34	1.56	1.42	0.08	1.28	1.54	1.43	0.08	1.25	1.43	1.32	0.06	0.97	1.12	1.06	0.04	0.81	1.22	0.95	0.08
$(Gd/Yb)_{UCC}$	1.16	1.26	1.20	0.06	1.03	1.30	1.18	0.09	0.99	1.30	1.14	0.09	0.93	1.18	1.08	0.07	0.80	1.32	1.02	0.11
$(La/Lu)_{UCC}$	1.33	1.64	1.43	0.11	1.24	1.57	1.35	0.09	1.13	1.42	1.29	0.10	0.89	1.11	1.01	0.06	0.70	1.21	0.91	0.09
$(La/Y)_{UCC}$	1.13	1.29	1.20	0.06	1.13	1.30	1.23	0.05	1.11	1.26	1.17	0.04	0.85	0.94	0.91	0.03	0.76	0.99	0.86	0.04
$(Gd/Lu)_{UCC}$	1.15	1.26	1.21	0.04	0.96	1.39	1.11	0.12	0.93	1.29	1.12	0.11	0.81	1.19	1.02	0.09	0.69	1.23	0.97	0.11

[a] *Min* minimum, *max* maximum, *SD* standard deviation, ∑*REE* total content of REEs, ∑*LREE* total content of LREEs (La to Eu), ∑*HREE* total content of HREEs (Gd to Lu, Y)

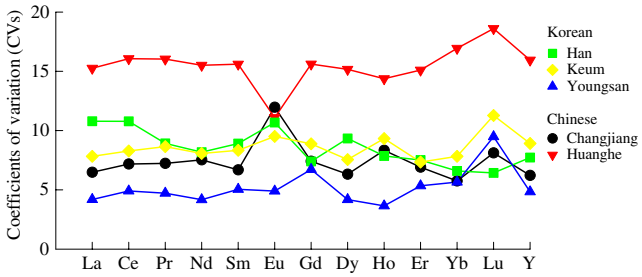

Fig. 2 Coefficients of variation (CVs) of REEs in Korean and Chinese river sediments. Note that most of the river sediments have CV values of less than 10%; however, Huanghe sediments have CV values higher than 15%, reflecting large variations in their REE contents (CV=standard deviation/mean value×100)

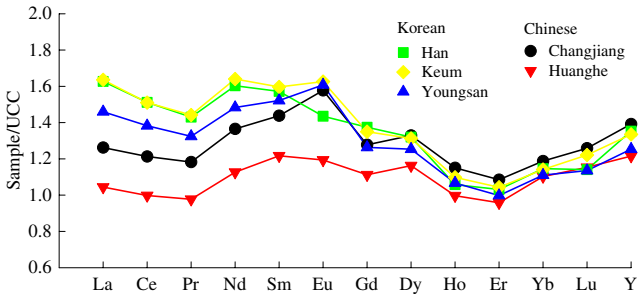

Fig. 3 UCC-normalized REE distribution patterns in Korean and Chinese river sediments. Note the pronounced LREE enrichment in Korean river sediments, and the convex patterns

fractionation ratios of REEs are notably higher in the Korean river samples than in their Chinese counterparts (for examples, see $(La/Lu)_{UCC}$ and $(La/Y)_{UCC}$ in Tables 2 and 3).

Pair diagrams of the linearly related LREEs and HREEs further illustrate the clear separation between the two groups of sediments; those from the Chinese rivers are enriched in HREEs (Fig. 4). Furthermore, plots of $(La/Lu)_{UCC}$ vs. $(La/Y)_{UCC}$, $(La/Yb)_{UCC}$ vs. $(Gd/Yb)_{UCC}$, and $(La/Y)_{UCC}$ vs. $(Gd/Lu)_{UCC}$ reveal that, in each case, the Chinese river sediments consistently group in the lower range of values for either one—$(La/Yb)_{UCC}$ vs. $(Gd/Yb)_{UCC}$—or both ratios (Fig. 5).

Discussion and conclusions

The higher LREE enrichment relative to HREE in samples of the study area is similar to findings for other major rivers in the world, such as the Amazon and the Mississippi (Goldstein and Jacobsen 1988), and those of previous

Table 3 Comparison of range, mean, and standard deviation (SD, μg/g), as well as fractionation ratios of REEs for Korean and Chinese river sediments

	Korean rivers (n=31)				Chinese rivers (n=60)			
	Min.	Max.	Mean	SD	Min.	Max.	Mean	SD
La	40.66	57.35	46.97	4.29	23.10	45.79	33.29	5.17
Ce	80.00	113.34	93.52	8.19	45.98	92.63	68.01	11.07
Pr	8.71	12.22	9.90	0.83	5.12	10.07	7.38	1.19
Nd	36.22	49.23	40.89	3.35	22.12	42.49	31.15	4.96
Sm	5.73	8.12	7.03	0.53	3.95	7.85	5.77	0.88
Eu	1.10	1.62	1.39	0.13	0.79	1.69	1.15	0.20
Gd	4.13	5.76	5.02	0.42	2.96	6.10	4.41	0.65
Dy	3.91	5.15	4.52	0.32	3.00	5.77	4.24	0.60
Ho	0.70	1.01	0.86	0.06	0.57	1.12	0.83	0.12
Er	2.11	2.74	2.35	0.16	1.60	3.15	2.29	0.32
Yb	2.24	2.83	2.49	0.17	1.79	3.69	2.48	0.36
Lu	0.32	0.49	0.38	0.04	0.23	0.59	0.38	0.06
Y	24.92	33.02	28.75	2.28	18.66	39.05	27.90	4.11
∑REE	212.10	291.18	244.07	19.94	130.34	256.56	189.31	29.23
∑LREE	173.37	240.86	199.70	16.95	101.28	200.00	146.76	23.34
∑HREE	38.73	50.32	44.37	3.27	29.06	59.42	42.55	6.10
∑LREE/∑HREE	4.26	4.81	4.50	0.16	3.15	3.80	3.44	0.16
$(La/Yb)_{UCC}$	1.25	1.56	1.39	0.09	0.81	1.22	0.99	0.08
$(Gd/Yb)_{UCC}$	0.99	1.30	1.17	0.08	0.80	1.32	1.03	0.10
$(La/Lu)_{UCC}$	1.13	1.64	1.34	0.11	0.70	1.21	0.94	0.09
$(La/Y)_{UCC}$	1.11	1.30	1.20	0.06	0.76	0.99	0.87	0.04
$(Gd/Lu)_{UCC}$	0.93	1.39	1.13	0.11	0.69	1.23	0.99	0.11

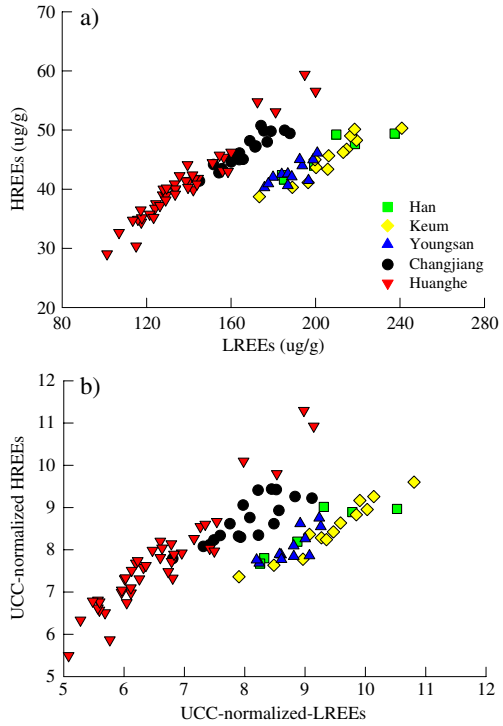

Fig. 4 Relationships between **a** HREE and LREE contents, and **b** UCC-normalized HREEs and LREEs contents for Korean and Chinese river sediments

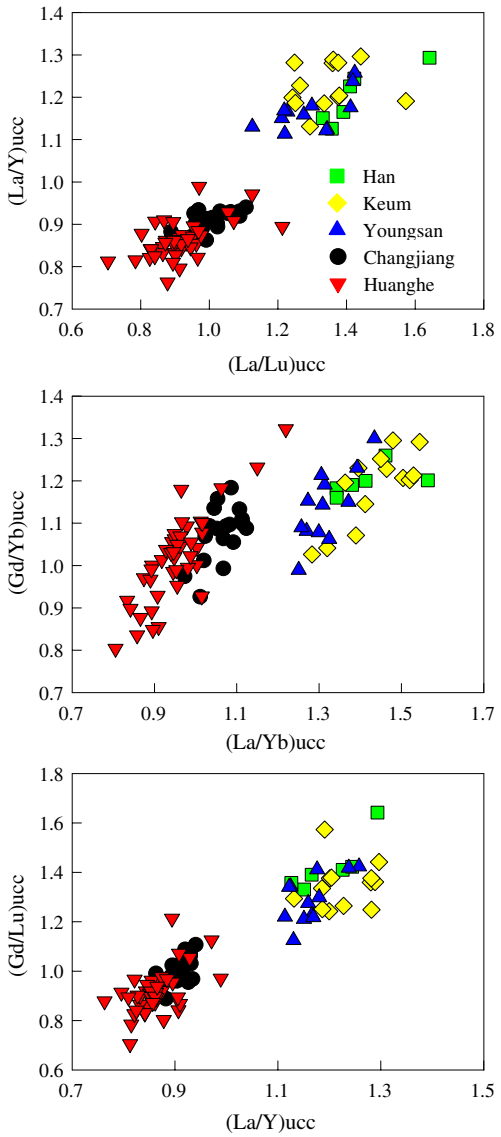

Fig. 5 Relationships between selected REE fractionation ratios for discriminating Korean and Chinese river sediments in the Yellow Sea

studies on bottom sediments of Chinese rivers (e.g., Zhang et al. 1998; Yang et al. 2002b). In coastal and river environments, especially compared with crust or shales, such relative enrichment of LREEs probably results from their high adsorption onto clay particles, while the HREEs are preferentially retained in solution (Byrne and Kim 1990; Ramesh et al. 1999; Caccia and Milero 2007).

The REE contents and UCC-normalized patterns of the Korean and Chinese bottom river sediments assessed in the present study are very similar to those recorded in the suspended matter of these rivers by Yang et al. (2003b) and Lin et al. (2008). This implies the existence of well-mixed weathering products from the drainage areas. Comparing the data for the Korean bottom river sediments with those of the corresponding source rocks (granite and granitic biotite for the Keum and Han rivers, respectively) of the Korean Peninsula reveals that their UCC-normalized REE patterns are very similar (Fig. 6a). In all cases, considerable LREE enrichment and HREE depletion relative to UCC are observed. Accordingly, the high ∑LREE/∑HREE fractionation ratios of the river sediments likely reflect the abundance of LREE-enriched granitic rocks in the Korean river drainage areas. The higher values of HREEs in the Korean sediment samples (compared to their source rocks), however, are probably a result of the relatively high degree of chemical weathering in the Korean drainage basins (Ryu et al. 2007). Such weathering promotes the mobility of HREEs (Sholkovitz et al. 1994), and would lead to a relative enrichment of HREEs in these river sediments.

The UCC-normalized REE distributions of the Changjiang sediments are very similar to those of the source rock (Jinshajiang clastic sediments) within the river catchment (Fig. 6b), indicating that source rock composition is the key factor influencing these bottom sediment REE patterns. In the case of the Huanghe sediments, however, the REE contents differ somewhat from those of the main potential Chinese loess source. The middle to heavy REE contents of the river sediments are generally lower than those of the loess, whereas REE fractionation is more apparent in the loess (Fig. 6b). This compositional dissimilarity between

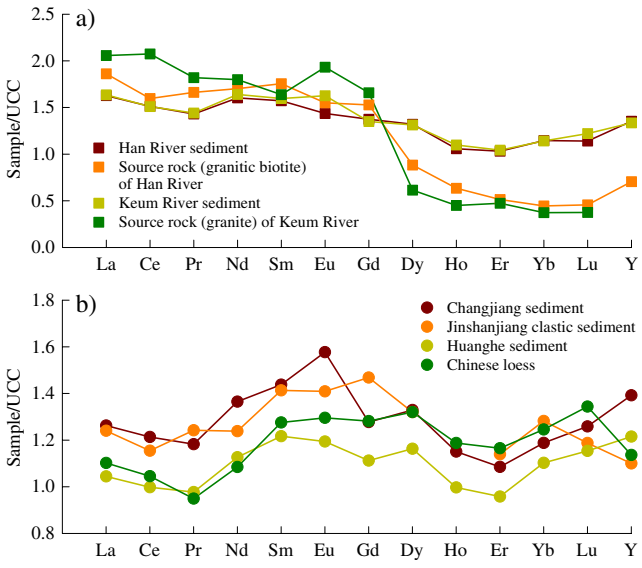

Fig. 6 Comparisons of UCC-normalized REE patterns between **a** Korean, and **b** Chinese river sediments and their source rocks. REE data for source rocks—granitic biotite, granite, Jinshajiang, and Chinese loess—are extracted from Lee et al. (2008), Park et al. (2007), Wang et al. (1994), and Wu et al. (1991), respectively

the Huanghe sediments and the source loess has been noted already by Yang et al. (2002b), with loess sample heterogeneity considered a likely explanation (Liu 1985; Zhang et al. 1990b). The geochemical composition of Chinese loess varies spatially, and the sand contents of the Huanghe sediments are generally higher than those of the loess (Liu 1985). Note that potential sources of Huanghe sediments include materials other than loess; REE-rich allanite and monazite are relatively abundant in loess, but rare in Huanghe sediments (Yang et al. 2002b). This would likely contribute to the mismatch in REE fingerprints between these river sediments and the loess. Nonetheless, in overall terms, the REE characteristics of the Chinese river sediments resemble those of their potential source rocks (Fig. 6b). Such compositional uniformity in river sediments and source materials indicates that weathering exerts only a minor influence on the REE signatures of these Chinese river sediments, despite chemical weathering being more pronounced in the Changjiang than in the Huanghe basin, where physical weathering dominates (Zhang et al. 1990a, 1990b; Yang et al. 2002b).

Systematic differences in REE compositions between Korean and Chinese river sediments may also be caused by their different mineralogy. A three-step sequential leaching of these river sediments (Song 2008) showed that the REE distribution patterns of bulk sediments are controlled largely by those of the residual phases, which are closely linked with clastic apatite and clay minerals (Ruttenberg 1992). In general, clay minerals are important reservoirs of REEs in riverine and marine muddy sediments; most of the REEs reside in the clay mineral lattice, whereas a small part is adsorbed onto the clay mineral surface. In addition, apatite contents in Chinese river sediments are low, and make only a small contribution to REE contents (Yang et al. 2002b). Therefore, clay mineral control on REEs in the study area is probably more important than heavy mineral control. Notably, the strong LREE enrichments in the Korean sediments are probably due to the variable abundance of chlorite (Song 2008). In fact, chlorite contents are much higher in Korean (14–19%) than in Chinese river-borne sediments (8–12%; Lim et al. 2003).

Another possible explanation for the higher LREE contents of Korean river sediments is the monazite level. Mineral phases such as monazite and zircon are enriched in LREEs, whereas minerals such as garnet and xenotime show more affinity for HREEs (e.g., Cullers et al. 1987). Recently, Jung et al. (2006) reported that monazite is one of the major constraints controlling the distribution patterns of REEs in the northern part of the East China Sea, influenced by sedimentary input from Korean rivers (even though monazite contents are very low in these sediments). Evidently, this aspect requires more detailed investigations in the Yellow Sea.

The strong positive Eu anomaly recorded in the Changjiang sediments confirms the findings of Yang et al. (2002b), and probably results from the high content of sphene mineral in these sediments (Zhou and Wang 1989; Sun 1990; Yang et al. 2002b). Compared to that of the Changjiang, the REE distribution pattern of the Huanghe sediments is relatively uniform, with REE contents and fractionations similar to those of the UCC, suggesting that these river sediments can be considered as model for the upper continental crust, and as reference for comparing REE compositions and fractionations of other surface sediments.

In conclusion, comparison with published data for the primary rock units within these Korean and Chinese river catchments shows that their main REE systematics are preserved in the river sediments. Thus, these REE fingerprints can be used as an important tool for identifying sediment origin, and associated sedimentation patterns, dispersal pathways, and relative contributions made by Korean and Chinese rivers to the fine-grained sediments of the Yellow Sea. Notably, high ∑LREE/∑HREE values in Yellow Sea sediments may reflect a high abundance of LREE-enriched Korean river sediments derived from granitic rocks, low values a high abundance of Chinese river sediments originating from sedimentary rocks, mainly carbonate and/or loess materials. Tracing the fate of these riverine source materials by means of REE signatures should prove helpful also in reconstructing their transport by paleocurrents (Liu et al. 2009). Furthermore, this

approach would nicely complement ongoing research dealing with other proxies of sediment provenance, such as magnetic properties (Zhang et al. 2008; Wang et al. 2009), and isotopic signatures, with obvious implications even for the management of heavy metal pollution in the coastal zone (e.g., Choi et al. 2007). Future work should focus on large-scale comparison between the sediment REE characters of these rivers and those on the shelf of the Yellow Sea and adjoining marginal seas.

Acknowledgements This study was supported by the research programs (grant no. PE98314, PE9830u) funded by the Korea Ocean Research and Development Institute (KORDI). We thank S. Lin and the journal editors for constructive comments.

References

Alexander CR, DeMaster DJ, Nittrouer CA (1991) Sediment accumulation in a modern epicontinental-shelf setting: the Yellow Sea. Mar Geol 98:51–72

Byrne RH, Kim KH (1990) Rare earth element scavenging in seawater. Geochim Cosmochim Acta 53:2645–2656

Caccia VG, Milero JF (2007) Distribution of yttrium and rare earths in Florida Bay sediments. Mar Chem 104:171–185

Chen JS, Wang FY, Li XD, Song JJ (2000) Geographical variations of trace elements in sediments of the major rivers in eastern China. Environ Geol 39:1334–1340

Chen XQ, Yan YX, Fu RS, Dou XP, Zhang EF (2008) Sediment transport from the Yangtze River, China, into the sea over the Post-Three Gorge Dam Period: a discussion. Quat Int 186:55–64

Cho YG, Lee CB, Choi MS (1999) Geochemistry of surface sediments off the southern and western coasts of Korea. Mar Geol 159:111–129

Choi M-S, Yi H-I, Yang SY, Lee C-B, H-J Cha (2007) Identification of Pb sources in Yellow Sea sediments using stable Pb isotope ratios. Mar Chem 107(2):255–274

Chough SK, Kim DC (1981) Dispersal of fine-grained sediments in the southeastern Yellow Sea: a steady-state model. J Sed Petrol 51:721–728

Cullers RL, Barrett T, Carlson R, Robinson B (1987) Rare earth element and mineralogical changes in Holocene soil and stream sediments: a case study in the wet mountains, Colorado, USA. Chem Geol 63:275–297

Elderfield H, Upstill-Goddard R, Sholkovitz ER (1990) The rare earth elements in rivers, estuaries, and coastal seas and their significance to the composition of ocean waters. Geochim Cosmochim Acta 54:971–991

Goldstein SJ, Jacobsen SB (1988) Rare earth elements in river waters. Earth Planet Sci Lett 89:35–47

Jiang FQ, Zhou XJ, Li AC, Li TG (2009) Quantitatively distinguishing sediments from the Yangtze River and the Yellow River using δ Eu_N-∑REEs plot. Sci China Series D Earth Sci 52(2):232–241

Jung HS, Lim DI, Yang SY, Yoo HS (2006) Constraints of REE distribution patterns in core sediments and their provenance, northern East China Sea (in Korean, with English abstract). Econ Environ Geol 39:39–51

Kim G, Yang H, Church TM (1999) Geochemistry of alkaline earth elements (Mg, Ca, Sr, Ba) in the surface sediments of the Yellow Sea. Chem Geol 153:1–10

Klaver GT, van Weering TCE (1993) Rare earth element fractionation by selective sediment dispersal in surface sediments: the Skagerrak. Mar Geol 111:345–359

Lan X, Wang H, Li R, Lin Z, Zhang Z (2007) Major elements composition and provenance analysis in the sediments of the south Yellow Sea. Earth Sci Frontiers 14(4):197–202

Lee HJ, Chu YS (2001) Origin of inner-shelf mud deposit in the southeastern Yellow Sea: Huksan Mud Belt. J Sed Res 71:144–154

Lee SG, Kim JK, Yang DY, Kim JY (2008) Rare earth element geochemistry and Nd isotope composition of stream sediments, south Han River drainage basin, Korea. Quat Int 176(177):121–134

Lim DI, Kim HN, Jung HS (2003) Geochemical-mineralogical characteristics of the pre-Holocene sediments in Haenam Bay, west coast of Korea. Geo-Mar Lett 22:210–217. doi:10.1007/s00367-002-0115-9

Lim DI, Jung HS, Choi JY, Yang S, Ahn KS (2006) Geochemical compositions of river and shelf sediments in the Yellow Sea: grain-size normalization and sediment provenance. Cont Shelf Res 26:15–24

Lim DI, Choi JY, Jung HS, Rho KC, Ahn KS (2007) Recent sediment accumulation and origin of shelf mud deposits in the Yellow Sea and East China Seas. Prog Oceanogr 73:145–159

Lin C, He M, Li Y, Yang L, Liu R, Yang Z (2008) Rare earth element content in the SPM of Daliao river system and its comparison with that in the sediments, loess and soils in China. J Rare Earths 26:414–420

Liu TS (1985) Loess and the environment (in Chinese). China Ocean, Beijing

Liu JP, Li AC, Xu KH, Velozzi DM, Yang ZS, Milliman JD, DeMaster DJ (2006) Sedimentary features of the Yangtze River-derived along-shelf clinoform deposit in the East China Sea. Cont Shelf Res 26:2141–2156

Liu J, Saito Y, Wang H, Yang Z, Nakashima R (2007) Sedimentary evolution of the Holocene subaqueous clinoform off the Shandong Peninsula in the Yellow Sea. Mar Geol 236:165–187

Liu J, Saito Y, Kong XH, Wang H, Zhao L (2009) Geochemical characteristics of sediment as indicators of post-glacial environmental changes off the Shandong Peninsula in the Yellow Sea. Cont Shelf Res 29:846–855. doi:10.1016/j.csr.2009.01.002

McLennan SM (1989) Rare earth elements in sedimentary rocks: influence of provenance and sedimentary processes. In: Lipin BR, McKay GA (eds) Geochemistry and mineralogy of rare earth elements. Reviews in Mineralogy, vol 21. Mineralogy Society of America, Washington, DC, pp 169–200

Milliman JD, Meade RH (1983) World-wide delivery of river sediment to the oceans. J Geol 91:1–21

Milliman JD, Shen HT, Yang ZS, Meade RH (1985) Transport and deposition of river sediment in the Changjiang estuary and adjacent continental shelf. Cont Shelf Res 4:37–45

Munksgaard NC, Lim K, Parry DL (2003) Rare earth elements as provenance indicators in North Australian estuarine and coastal marine sediments. Estuarine Coastal Shelf Sci 57:399–409

Nittrouer CA, DeMaster DJ, Kuehl SA, McKee BA, Thorbjarnarson KW (1984) Some questions and answers about the accumulation of fine-grained sediment in continental margin environments. Geo-Mar Lett 4:211–213. doi:10.1007/BF02281708

Nohara M, Yokoto S, Saito Y (1999) Sr-Nd isotopic and trace elements constrained on the origin of the sediments in the Yellow and East China Seas. In: Saito Y, Ikehara K, Katayama H (eds) Proc Int Worksh Sediment Transport and Storage in Coastal Sea-Ocean Systems. Tsukuba, Japan, pp 123–127

Park SC, Lee HH, Han HS, Lee GH, Kim DC, Yoo DG (2000) Evolution of late Quaternary mud deposits and recent sediment budget in the southeastern Yellow Sea. Mar Geol 170:271–288

Park CS, Yoon SO, Hwang S (2007) Properties and provenance of loess-paleosol sequence at the Daebo Granite area of Buan, Jeonbuk Province, South Korea (in Korean, with English abstract). J Korea Geogr Soc 42:898–913

Ramesh R, Ramanathan AL, James RA, Subramanian V, Jacobsen SB, Holland HD (1999) Rare earth elements and heavy metal distribution in estuarine sediments of east coast of India. Hydrobiologia 397:89–99

Ren ME, Shi YL (1986) Sediment discharge of the Yellow River (China) and its effect on the sedimentation of the Bohai and the Yellow Sea. Cont Shelf Res 6:785–810

Ruttenberg KC (1992) Development of a sequential extraction method for different forms of phosphorus in marine sediments. Limnol Oceanogr 37:1460–1482

Ryu JS, Lee KS, Lee SG, Lee D, Chang HW (2007) Seasonal and spatial variations of rare earth elements in rainwaters, river waters and total suspended particles in air in South Korea. J Alloys Compounds 437:344–350

Sholkovitz ER, Landing WM, Lewis BL (1994) Ocean particle chemistry: the fractionation of rare earth elements between suspended particles and seawater. Geochim Cosmochim Acta 58:1567–1579

Song YH (2008) Provenance of fine-grained surface sediment in the Yellow Sea using REE (in Korean, with English abstract). MSc Thesis. Chungnam National University, Seoul

Su C-C, Huh C-A (2002) ^{210}Pb, ^{137}Cs and ^{239,240}Pu in East China Sea sediments: sources, pathways and budgets of sediments and radionuclides. Mar Geol 183(1/4):163–178

Sun BY (1990) Detrital mineral assemblages in the Huanghe, Changjiang and Zhujiang River Delta sediments (in Chinese, with English abstract). Mar Geol Quat Geol 10:23–34

Taylor SR, McLennan SM (1985) The continental crust: its composition and evolution. Blackwell, Oxford

Wang XR, Lu JH, Peng F, Tu Q, Tian LQ, Dai LM, Li Z, Chen YJ (1994) Geochemical characteristics and environmental background values of rare earth elements in river water and sediments from the Jinshajiang river system (in Chinese, with English abstract). Acta Scientiae Circumstantiae 14:168–176

Wang H, Zhang X, Lan X, Zhang Z, Lin Z, Zhao G (2007) Geochemistry characteristics of sediment and provenance relations of sediments in core NT1 of the south Yellow sea. J China Univ Geosci 18(4):287–298

Wang Y, Yu Z, Li G, Oguchi T, He H, Shen H (2009) Discrimination in magnetic properties of different-sized sediments from the Changjiang and Huanghe Estuaries of China and its implication for provenance of sediment on the shelf. Mar Geol (in press). doi:10.1016/j.margeo.2009.02.008

Wu MQ, Wen QZ, Pan JY, Diao GY (1991) Rare earth elements of Malan loess from the middle reaches of the Huanghe River. Chinese Sci Bull 36:1380–1385

Xu K, Milliman JD (2009) Seasonal variations of sediment discharge from the Yangtze River before and after impoundment of the Three Gorges dam. Geomorphology 104(3/4):276–283

Yang ZS, Liu JP (2007) A unique Yellow River-derived distal subaqueous delta in the Yellow Sea. Mar Geol 240:169–176

Yang SY, Youn J (2007) Geochemical compositions and provenance discrimination of the central south Yellow Sea sediments. Mar Geol 243:229–242

Yang SY, Li CX, Jung HS, Lee HJ (2002a) Discrimination of geochemical compositions between the Changjiang and the Huanghe sediments and its application for the identification of sediment source in the Jiangsu coastal plain, China. Mar Geol 186(3/4):229–241

Yang SY, Jung HS, Choi MS, Li CX (2002b) The rare earth element compositions of the Changjiang (Yangtze) and Huanghe (Yellow) river sediments. Earth Planet Sci Lett 201:407–419

Yang SY, Jung HS, Lim DI, Li CX (2003a) A review on the provenance discrimination of sediments in the Yellow Sea. Earth-Sci Rev 63:93–120

Yang SY, Li CX, Lee CB, Na TK (2003b) REE geochemistry of suspended sediments from the rivers around the Yellow Sea and provenance indicators. Chinese Sci Bull 48:1135–1139

Yang SY, Jiang SY, Ling HF, Xia XP, Sun M, Wang DJ (2007) Sr-Nd isotopic compositions of the Changjiang sediments: implications for tracing sediments sources. Sci China Series D Earth Sci 50 (10):1556–1565

Zhang J, Huang WW, Liu MG, Zhou Q (1990a) Drainage basin weathering and major element transport of two large Chinese rivers (Huanghe and Changjiang). J Geophys Res 95:13277–13288

Zhang J, Huang WW, Shi MC (1990b) Huanghe (Yellow River) and its estuary: sediment origin, transport and deposition. J Hydrol 120:203–223

Zhang C, Wang L, Zhang S (1998) Geochemistry of rare earth elements in the mainstream of the Yangtze River, China. Appl Geochem 13:451–462

Zhang W, Xing Y, Yu L, Feng H, Lu M (2008) Distinguishing sediments from the Yangtze and Yellow Rivers, China: a mineral magnetic approach. Holocene 18(7):1139–1145

Zhou LD, Wang YC (1989) REE geochemical characteristics of apatite, sphene and zircon from alkaline rocks. Chinese J Geochem 8:245–253

Zhu W, Kennedy M, de Leer EWB, Zhou H, Alaerts GJFR (1997) Distribution and modeling of rare earth elements in Chinese river sediments. Sci Total Environ 204:233–243

Journal of Coastal Research	SI 56	732 - 736	ICS2009(Proceedings)	Portugal	ISSN 0749-0258

Sea-cliff erosion and retreat in semi-enclosed macrotidal embayment: Hampyung Bay, west coast of Korea

D.I. Lim† J.Y. Choi‡ and H.S. Jung†

†Korea Ocean Research and Development Institute, Ansan, P.O. Box 29, Seoul 425-600, Korea
oceanlim@kordi.re.kr

‡ Depart. of Oceanography, Kunsan National University, Kunsan 573-701, Korea
jinyong@kunsan.ac.kr

ABSTRACT

Lim, D.I., Choi, J.Y. and Jung, H.S., 2009. Sea-cliff erosion and retreat in semi-enclosed embayment: macrotidal Hampyung Bay, west coast of Korea. Journal of Coastal Research, SI 56 (Proceedings of the 10th International Coastal Symposium), pg ï pg. Lisbon, Portugal, ISBN

The coastline of semi-enclosed, macrotidal Hampyung Bay, on the west coast of Korea, was monitored seasonally to investigate sea-cliff retreat processes. The long-term retreat rate of the coastline was measured by comparing aerial photographs taken in 1976 and 1990. The coastline of the bay has an irregular, saw-tooth shape and is characterized by poorly consolidated soil, sea cliffs, and steep slopes. Unusual geomorphic features (remnants of former sea cliffs and ñisland stacksò) on the tidal flat and beach near the sea cliffs, together with the unique, saw-tooth-like coastline configuration, indicate that the coastline has been undergoing sea-cliff erosion for hundreds of years. Quantification of sea-cliff retreat rates yields average cliff retreat rates of 1ï2 m/yr between 1976 and 1990; these values agree with estimates based on short-term field measurements (0.5ï2.0 m/yr). Sea-cliff erosion in the semi-enclosed bay system probably results from episodic storm/typhoon surges affecting the poorly consolidated soil cliffs. A cliff-retreat model for the study area suggests that the sea cliffs are continuously retreating through a cyclic process: erosion of the cliff base during episodic, high-energy events (mainly winter storms) forms notches; gravitational failure produces soil talus at the base of the cliffs; and talus is then removed by disintegration. Especially, high sea-level episodes by a relatively higher tidal range during summer may be a key factor in the removal of soil talus, which accelerates sea-cliff erosion.

ADITIONAL INDEX WORDS: *Soil sea-cliff, Seasonal change, Macrotidal flat*

INTRODUCTION

The west coast of Korea (eastern coast of the Yellow Sea) is one of the worldôs most dynamic ria-coastal regions, with strong monsoonal typhoons and frequent storms that generate severe waves and surge causing coastal erosion (JUN, 1995; PARK, 1996; HYUN et al., 2001). Over the past several decades, this area has experienced coastline recession (KWON, 1981, 1983), even though the semi-enclosed embayment system protects the coastline from the strong wave action of the open sea. Hampyung Bay is typical of western Korean coastal embayments. It is a semi-enclosed, gourd-shaped bay, with a 3.5 m average tidal range and large, muddy tidal flats (Fig. 1). The tidal flats, extensively developed along the margins of the bay, contain scattered, small sand bars and cheniers. The monsoonal climate is characterized by a cold, dry wind from the north to northeast in autumn and winter, and warm, humid summer wind from the SSE that occasionally intensifies into typhoons (RYU, 1998). On average, more than ten typhoons per year occur in East Asia, of which three or four affect the Korean coasts with heavy rain and severe wind. The winter season (November ~ March) is the time of most intense coastal damage. Storm surges (>13.9 m/sec maximum wind speed) occur 28.8 days per year, most of which are during winter (PARK, 1996).

The coast of Hampyung Bay is characterized by unstable sea cliffs that consist predominantly of deeply weathered soil or granite gneiss. The sea cliffs are retreating episodically, generally when high tide and storm waves coincide (RYU et al., 1999; CHANG et al., 1999). As in many other bay areas, homes, roads and agricultural fields along the Hampyung Bay coastline have been damaged over the last two decades. Quantifying erosion rates would help in establishing safe construction setbacks, settling property disputes, and informing land-use changes. However, only very limited data are available to quantify the coastal retreat process. In this study, sea-cliff profiles were systematically measured along the coastline of Hampyung Bay to understand their retreat processes, and long-term recession rates of the sea cliffs were quantitatively estimated using historical aerial photogrammetry.

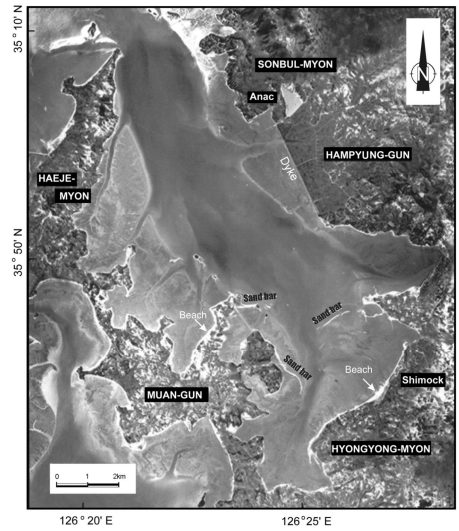

Figure 1. Aerial photograph of the entire Hampyung Bay. Note that its morphology is characterized by saw-tooth-shaped coastline reflecting active sea-cliff erosion and retreat.

MATERIALS AND METHODS

To determine seasonal changes in cliff profiles, field measurements were conducted at four locations from April 2001 to March 2002 (Fig. 2), using a precision leveling device (SOKKIA SET2110R Model) with an accuracy of ±5 mm. The measurements were repeated at approximately three-month intervals. The longer-term cliff retreat rate was estimated using 1:20,000-scale aerial photographs from 1976 and 1990. The distortions inherent to aerial photography, such as tilt displacement and relief displacement (e.g., KIM *et al*., 1998), were corrected using the direct linear transformation (DLT) technique suggested by ABDEL-AZIZ and KARARA (1971).

In historical shoreline mapping studies, the shoreline is defined as the high water line (HWL) (DOLAN *et al*., 1978; SHOSHANY and DEGANI, 1992). The HWL in a typical beach environment is assumed to indicate sea-surface elevation (i.e., Z=0). In contrast, the shoreline associated with sea cliffs tends to have irregular elevations due to spatial variations in sea-cliff heights and to be strongly affected by erosion. Considering that the height of most sea cliffs in Hampyung Bay is less than 3ï 5 m above mean high-water level, it is reasonable to adopt the base of the sea cliffs as the HWL.

To rectify each aerial photograph, DLT coefficients must be determined using at least six ground control points (GCPs) that are common to aerial photographs of different years. The aerial photographs were digitized at a resolution of 600 dpi using a non-metric scanner, producing a pixel size of 42 μm, which is equivalent to 0.85 m on the ground. Ten control points were selected from the two digitized photographs, and their image coordinates were read with an accuracy of one pixel. Horizontal ground coordinates of the control points were also obtained from a 1:5,000-scale digital map published by the Korea National Geographic Institute. Vertical ground coordinates of the GCPs were estimated by interpolation of contour lines. Both image and ground coordinates of the GCPs were integrated into the equation suggested by ABDEL-AZIZ and KARARA (1971), and then 11 DLT coefficients were evaluated by a least-square method. To assess the rectification process, root-mean square (RMS) errors between observed and calculated ground coordinates of GCPs were estimated.

RESULTS

Coastline configuration and seasonal cliff profiles

The coastline of Hampyung Bay is characterized by a peculiar saw teeth-shaped configuration (Fig. 2), indicating that the coastal area is dynamically changing over time scales of hundreds of years. Most of coastline comprises steep sea-cliffs composed of the soft, reddish brown soil and/or the poorly-consolidated, weathered granite gneiss. These cliffs are consistently very steep, forming vertical angles about 10˚ in general, and their height varies from approximately 5ï 20 m with a typical cliff height of about 10 m. At the base of the cliff, small pocket beaches have developed approximately 1 m above mean sea-level.

The coastline of Hampyung Bay is characterized by a peculiar saw-tooth-shaped configuration (Fig. 2) that is a function of its rapid evolution at a time-scale of hundreds of years. Most of the coastline consists of steep sea cliffs composed of soft, reddish-brown soil and/or deeply weathered granitic gneiss. The cliffs are consistently very steep (generally about 10° from vertical), with heights from 5 to 20 m (typically ~10 m). At the base of the cliff, small pocket beaches have developed approximately 1 m above mean sea level. In most cases, the beaches are gently sloping surfaces that extend 30ï 70 m seaward from the cliff and consist of angular, coarse sand supplied by erosion of the sea cliffs. Striking geomorphological features in Hampyung Bay are basement rock debris and ñisland stacksò (PETHICK, 1984) exposed on pocket beaches and high tidal flats near the sea cliffs. These are probably relicts of the rapidly retreating coastline and may mark its former position. Artificial dykes constructed to protect farms and buildings from coastal erosion occupy over 60% of the Hampyung Bay coastline (Fig. 2).

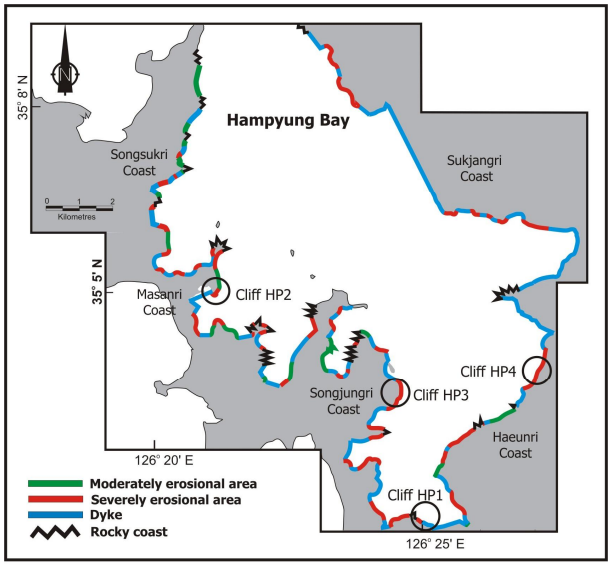

Figure 2. Map showing areas of costal erosion. Most of coastline is experiencing active erosion. Four circles (Cliff HP1 to 4) indicate the locations of sea cliff monitored in this study.

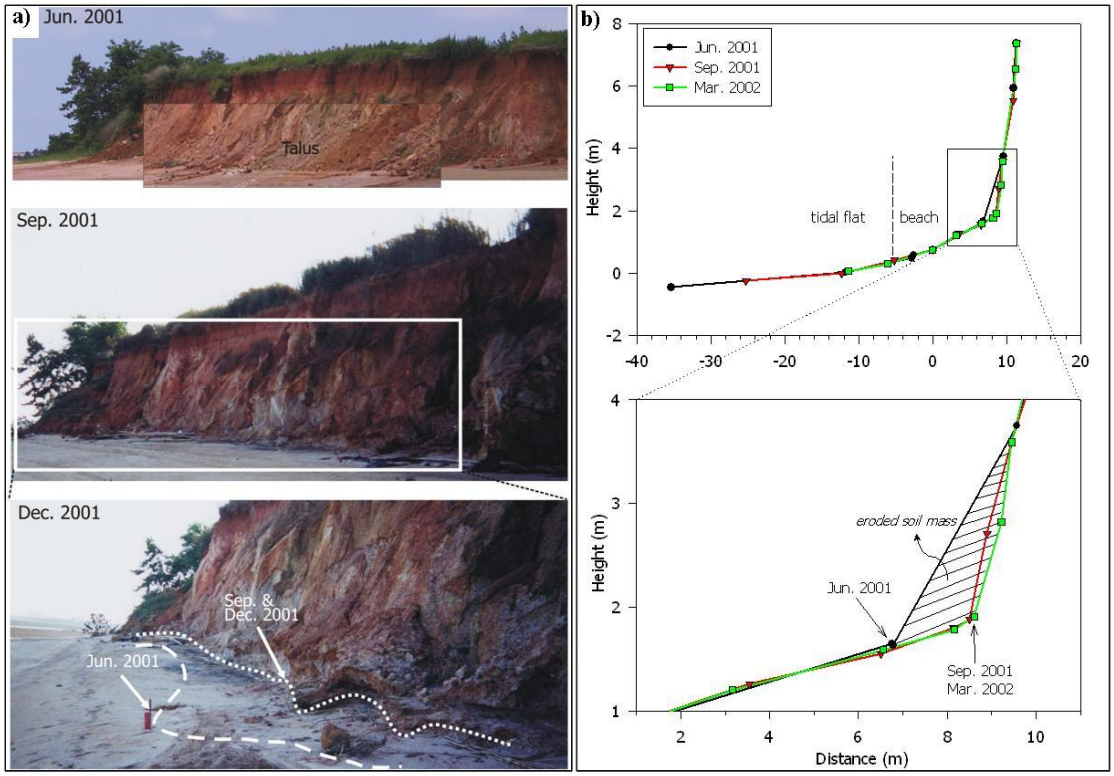

Figure 3. (a) Time-series field photographs and (b) seasonal variations of the sea-cliff profile at site HP2 (sea Fig. 2). The zero point in X- and Y- axis signifies a datum point installed near the sea cliff. Note the formation and disappearance of soil talus at the cliff base.

The sea cliffs measured (Fig. 2) were 3ï 7 m high and 30ï 50 m long and composed of unstable, soft soil (Fig. 3). The sea-cliff faces are extremely irregular due to the falling of jointed blocks. Detritus from the cliffs accumulates on pocket beaches, which consist of angular, coarse sand and gravel similar to those in the sea-cliff soil. Abundant soil talus was present at the cliff base in June 2001, but was absent in April 2001 (Fig. 3), suggesting that cliff-collapse events take place in spring to early summer. Soil talus was absent in September 2001, indicating that all of the talus material had been removed during the summer, steepening the cliff profile. Profiles for December 2001 and March 2002 indicate that cliffs are steeper in winter than at other times of year, but experience only slight, local erosion. In winter profiles, characteristic notches at the bases of some cliffs probably resulted from strong wave action. This undercutting of the sea-cliff base appears to be episodic, commonly occurring during severe storms in association with elevated wave energy and heavy rainfall. The horizontal retreat distance of the sea cliffs between April 2001 and March 2002 ranged from 0.5 to 2 m.

Long-term sea-cliff retreat rate

In general, coastal erosion rates are determined by dividing the difference between a recent shoreline position (as seen on a recent map) and a past shoreline position (as seen on historical aerial photographs) by the time interval between the two end points. Using an intersection process of the DLT equation, image coordinates of about 1 km shoreline section of Haeunri coast, located at the southeastern part of the Hampyung Bay (see Fig. 2), are transformed into ground coordinates, assuming that elevation of shoreline is mean sea level. The results indicate RMS errors in the (X, Y) coordinates of 1.7 and 1.9 m for 1976 and 1.9 and 2.0 m for 1990. Euclidean distances of the RMS errors are 2.6 m for 1976 and 2.8 m for 1990. The errors are no more than three pixels of the digital images and thus the outcome of the GCP measurements is satisfactory.

The coastlines of the Haeunri area derived from the aerial photographs (Fig. 4) show that the 1990 coastline was landward of the 1976 shoreline, indicating a retreat. The shoreline shifted by between 17 and 28 m (mean 24.9 m) over 14 years; therefore, the annual landward retreat of sea-cliff shorelines on the Haeunri coast can be estimated to be in the range of 1 to 2 m. Considering the degree of GCP error ranges, the shoreline changes are significant. The sea-cliff recession rate corresponds to the value of measured retreat (0.6~2.1 m/yr in range, 1.4 m/yr in average) in the same region (CHANG et al., 1999), proving the effectiveness of aerial monitoring.

DISCUSSION

The Hampyung Bay coastline is characterized by steep cliffs formed in soft soil and/or deeply weathered rocks. The saw-tooth-shaped configuration, unique geomorphic characteristics (erosional debris of paleo-sea cliffs and island stacks), and the presence of many artificial dykes indicate that the sea-cliff coastline has been undergoing active sea-cliff erosion for hundreds of years. Aerial photograph analysis indicates that the average retreat rate of the coastline, especially along the Haeunri coast, is high, ranging from 1 to 2 m/yr. This range is comparable with that of other dynamic coasts under continual erosion, such as coastlines in southern Portugal (DIAS and NEAL, 1992) and New Zealand (MOON and HEALY, 1994).

Sea-cliff erosion in previous models is generally controlled by sea-level, sea-cliff composition, degree of wave exposure, and the presence and width of a protective beach or tidal flat (SUNAMURA, 1982; MOON and HEALY, 1994; DAVIDSON-ARNOTT and OLLERHEAD, 1995; PHILLIPS, 1999). Recently, a model on the erosion of cohesive clay coasts in macro-tidal environment, which differs from previous developed models, was developed to examine relationships between variables that affect the erosion and development of clay coasts, including wave generated bottom shear stresses, morphodynamics of beach, wave conditions and friction factors, tide and water depths etc. (TRENHAILE, 2009).

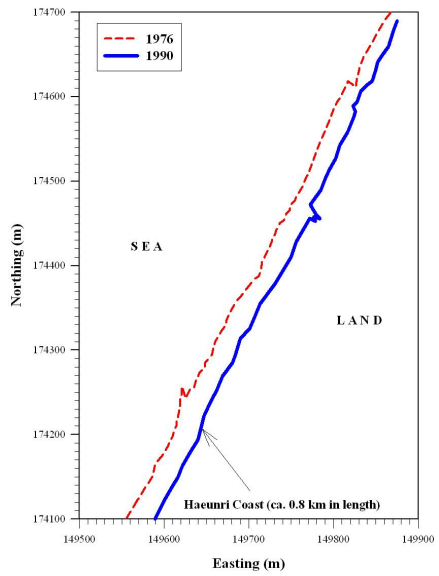

Figure 4. Map showing the 1976 and 1990 shoreline positions calculated by photogrammetry using aerial photographs.

Hampyung Bay is a semi-enclosed embayment with a narrow entrance and an extensive tidal flat, and thus fair-weather waves are probably not a dominant factor in coastline erosion. Sea-cliff erosion in Hampyung Bay is most likely the result of the combined effects of episodic, severe typhoons and storm surges with weak resistance of the soil cliff. A cliff-retreat model for the study area is proposed on the basis of field observations and in terms of an ideal, homogeneous soil cliff with no geologic structure and free of human influence. Fig. 5 schematically depicts the cyclic retreat processes. Profile I is characterized by an unstable sea cliff with a steep slope, and post-dates episodic high-energy events such as winter storm surges. The unstable sea cliff of Profile I breaks apart by mass wasting, resulting in Profile II, which has talus at its base consisting of the broken soil blocks and other debris. Profile II is sigmoidal, with a shape determined by the size and total volume of the talus blocks and the height of the cliff. Monitoring data show that sea-cliff collapse and talus formation take place predominantly in spring when the frozen soil of the cliff thaws.

Soil talus formed in spring disintegrates completely during summer, leaving a steep sea-cliff profile once again (Profile III). Considering that there were no storms during the observation interval, talus disintegration near the cliff base may be attributable to a relatively higher tidal range during the summer. Spring tides in summer are more than 0.5 m higher than those in the spring months when the talus forms (RYU, 1998). This suggests that the talus is probably demolished by gradual erosion and weak wave action during the highest summer tides, rather than by intermittent storms. If Profile III is reached at the beginning of summer, it can be maintained until the fall and winter seasons, when strong waves once again become common. New wave-cut notches are formed by strong winter storm surges, and then the summer cliff profile rapidly changes to Profile IV, in which only rare blocks fall from the middle part of the profile (just above the notch). Profile I is reached, and a new cycle starts. Consequently, the sea-cliffs are continuously retreating with the following cyclic process: erosion of cliff base (formation of the notches) after episodic high energy events (mainly winter storms) → gravitational landslide of mass wasting and formation of talus → removal of talus causing retreat of sea-cliff. The cycle model proposes seasonal or regular retreat that takes place without significant wave effects. The time span of the entire cycle is quite variable, depending on the beach profile, wave conditions, and storm frequency. This schematic model and interpretation for cliff evolution awaits confirmation based on more long-tem field measurement data.

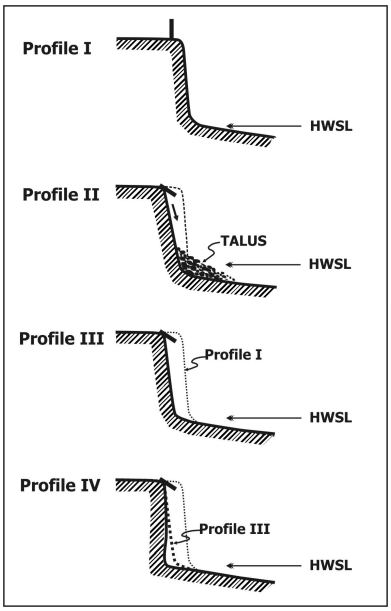

Figure 5. Schematic diagram showing the evolution of sea-cliff profile on the coast of Hampyung Bay. The coastline retreats incrementally as soil talus is repeatedly shed from the cliff and removed.

CONCLUSION

In semi-enclosed Hampyung Bay, west coast of Korea, saw-tooth shaped sea-cliffs have been annually retreated landward in the range of 1-2 m on the basis of short-term filed measurement and long-term aerial monitoring data. According to our cliff evolution model, the sea cliffs are continuously retreating according to the following cyclic series of processes: erosion of the cliff base (formation of notches) during episodic high-energy events (mainly winter storms); mass wasting and formation of talus; and removal of talus causing retreat of the sea cliff. The rapid coastline retreat rate is a function of seasonally repeated, external processes acting on cliff-forming material that has little resistance to erosion of any sort.

LITERATURE CITED

ABDEL-AZIZ, Y.I. and KARARA, H.M., 1971. Direct linear transformation from comparator coordinates into object space coordinates in close-range photogrammetry. *Proceedings of the ASP/UI symposium on close-range photogrammetry* (Urbana, Illinois), pp. 1-18

CHANG, J.H.; KIM, Y.S.; CHO, Y.G., 1999. Tidal-flat sedimentation in a semienclosed bay with erosional shorelines: Hampyung Bay, west coast of Korea (in Korean with English Abstract). 「*The Sea*」*Journal of Korean Society of Oceanography*, 4, 117-126.

DAVIDSON-ARNOTT, R.G.D. and OLLERHEAD J., 1995. Nearshore erosion on a cohesive shoreline. *Marine Geology*, 122, 349-456

DIAS, J.M.A. and NEAL, W.J., 1992. Sea cliff retreat in southern Portugal: Profiles, Processes, and Problems. *Journal of Coastal Research*, 8, 641-654

DOLAN, R.; HAYDEN, B.; HEYWOOD, J., 1978. A new photogrammetric method for determining shorline erosion. *Coastal Engineering*, 2, 21-39

HYUN, S.K.; LEE, D.Y.; JEON, K.C., 2001. Characteristics of typhoons between 1951 and 2000 in Korean Peninsular: Statistical approach. *Proceedings of the natural disaster protection workshop* (Pocehon, Korea), pp. 44-50.

JUN, D., 1995. Coastal erosion models with oceanic forcing (in Korean with English Abstract). *Ocean Research*, 17, 41-58.

KIM, B.O.; CHO, H.Y.; LIM, D.I.; YOON, G.L.; OH, I.S.; PARK, Y.A., 2008. Nearshore wave measurement using single-video images of buoy motions. *Journal of Coastal Research*, 24, 1481-1486

KWON, H.J., 1981. Topography of the Taean and Anmyundo coastlines in the west coast of Korea (in Korean). *Bulletin of University of Korea*, 6, 261-287

KWON, H.J., 198. Coastal erosion in west coast of Korea (in Korean). *Bulletin of University of Korea*, 18, 137-155

MOON, V.G. and HEALY, T., 1994. Mechanisms of coastal cliff retreat and hazard zone delineation in soft flysch deposits. *Journal of Coastal Research*, 10: 663-680

PARK, Y.A., 1996. Coastal Typhoon Deposit in Hampyung Bay, Southwest Coast of Korea (in Korean with English Abstract). *Journal of Korean Society of Oceanography*, 31, 32-36

PHILLIPS, J.D., 1999. Event timing and sequence in coastal shoreline erosion: Hurricanes Bertha and Fran and the Neuse Estuary. *Journal of Coastal Research*, 15, 616-623

RYU, S.O., 1998. Sedimentary environments and Stratigraphy of Hampyung Bay, southwestern Korean coast. Gwangju, Korea: Chonnam National University, Ph.D. thesis, 248p.

RYU, S.O.; YOO, H.S.; LEE, J.D., 1999. Seasonal variation of surface sediments and accumulation rate on the intertidal flats in Hampyung Bay, southwestern coast of Korea (in Korean with English Abstract). 「*The Sea*」*Journal of Korean Society of Oceanography*, 4, 127-135

SHOSHANY, M. and DEGANI, A., 1992. Shoreline detection by digital image porcessing of aerial photography. *Journal of Coastal Research*, 8, 29-34

SUNAMURA, T., 1982. A predictive model for wave-induced cliff erosion with application to Pacific coasts of Japan. *Journal of Geology*, 90, 167-181

TRENHAILE, A.S., 2009. Modeling the erosion of cohesive clay coast. *Coastal Engineering*, 56, 59-72

ACKNOLEDGEMENT

This work was supported by the KORDI Research Fund (Grant No. PE9830U) in Korea.